A SPECTROSCOPIC INVESTIGATION OF AN ARGON GLOW DISCHARGE

ROBERT C. AUSTIN
and
HARRY C. SCHRADER, JR.

A SPECTROSCOPIC INVESTIGATION OF AN ARGON GLOW DISCHARGE

* * * * *

Robert C. Austin

and

Harry C. Schrader Jr.

A SPECTROSCOPIC INVESTIGATION OF AN ARGON GLOW DISCHARGE

by

Robert C. Austin
Lieutenant, United States Navy

and

Harry C. Schrader Jr.
Lieutenant, United States Navy

Submitted in partial fulfillment of
the requirements for the degree of

MASTER OF SCIENCE
IN
PHYSICS

United States Naval Postgraduate School
Monterey, California

1963

A SPECTROSCOPIC INVESTIGATION OF AN ARGON GLOW DISCHARGE

by

Robert C. Austin

and

Harry C. Schrader Jr.

This work is accepted as fulfilling
the thesis requirements for the degree of
MASTER OF SCIENCE
IN
PHYSICS
from the
United States Naval Postgraduate School

ABSTRACT

The positive column of an Argon glow discharge was observed through a Fabry-Perot interferometer with a prism spectrograph in order to determine if a Doppler shift occurs. No Doppler shifts were observed; however, further refinements in equipment and technique are required before it can be reported that no Doppler shifts exists.

Feasibility of removable end plate construction of discharge tubes was investigated and future design parameters were specified.

Methods for obtaining emitter radial distributions from spectroscopic intensity measurements were investigated. In lieu of experimental data, artifical intensity measurements were used as inputs to the Control Data Corporation 1604 digital computer in order to compare and to determine the sensitivity of these methods.

TABLE OF CONTENTS

LIST OF ILLUSTRATIONS

1. Introduction

1.1 History

During the past century investigations have been made of the field we currently call plasma physics. It was first termed the physics of gas discharges, then with the introduction of electronics it was called gaseous electronics. The term plasma was coined in 1920 by Irving Langmuir[1] to denote a gas discharge in which quasi-neutrality is maintained, and in which a visible glow is apparent.

Unfortunately, there is still no standard, all inclusive, definition for the term plasma. It may be defined as a neutral collection of electrons and positive ions; however this is an over-simplification. The true definition must be considered with respect to the application of the plasma and the environment under which it exists. Under these restrictions, the plasma may be defined in terms of Debye length, a characteristic linear dimension; electron and/or density temperature, or degree of ionization.

Much of our knowledge of plasmas has been obtained using spectroscopic diagnostic techniques. Using these methods, information about the plasma constituents, temperatures, densities, and particle velocities has been obtained. Recently, microwave, probe, and other non-spectroscopic methods have been perfected. Under some circumstances they provide more accurate data than optical devices, but they have one common fault, they perturb the plasma.

As a result of the discovery of moving striation in 1874 by Wullner[2] in glow discharges, many studies of this phenomenon have been undertaken. Moving striations are "the alternate bands of darkness and luminosity traveling through the positive column of gas glow discharges in Mercury and inert gases." [3]

1.2 Glow Discharges.

A large number of studies have been made of glow discharges; as a result, the characteristic regions of this type gas discharge have been classified according to the standard nomenclature shown in figure 1a.

A glow discharge which is maintained by electrons produced at the cathode by a combination of positive-ion bombardment and electron emission from the cathode filament is called a hot cathode discharge. Current within the discharge is maintained by placing a potential of several hundred volts across the discharge tube.

The positive column is the region of our interest. It is the ionized region that extends from the Faraday dark space to the anode glow region. From figures 1b, c, d, [4] it is obvious that this region is characterized by high light intensity, a low potential drop, and low electric field strength. The visible glow from this region comes from transitions of bound electrons in the Argon atoms, or from free electron entering or leaving bound atomic states. There is no evidence that similar interactions are occurring with the Argon positive ions.[5] The physically obvious characteristics of the positive column are heavily dependent on many parameters such as tube geometry, gas pressure, discharge current, supplied voltage, cathode temperature, and type of gas.

1.3 Previous Experimental Work.

Far too many experiments have been conducted on moving striations during this century to be reviewed in this paper. An excellent summary of early works was made by J. J. Thompson[2]; the work done in the period 1920-1956 is outlined by A. W. Cooper[3] and G. Francis[6]. However, two

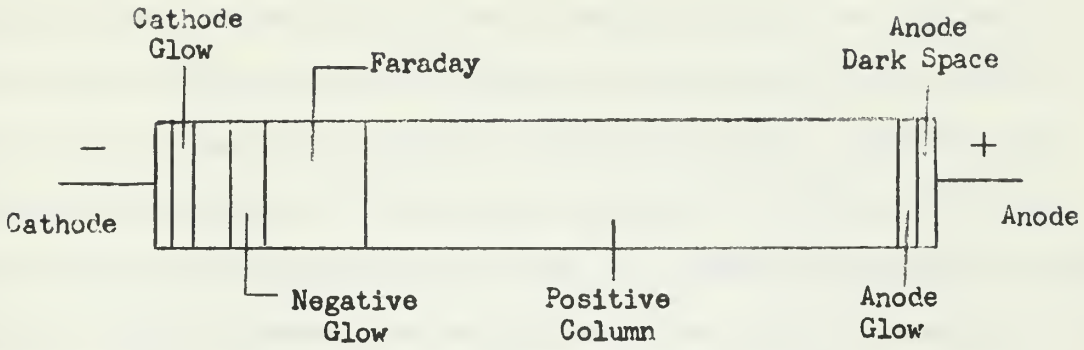

Figure 1a. Glow Discharge Classification

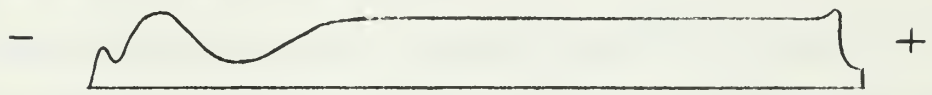

Figure 1b. Light Intensity

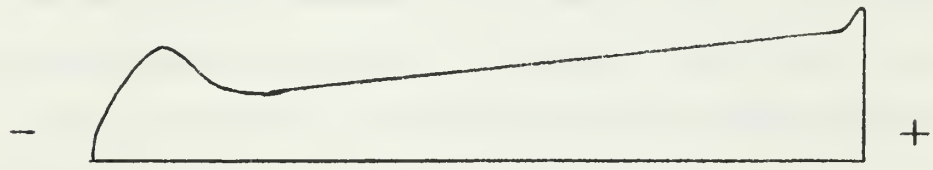

Figure 1c. Potential Distribution

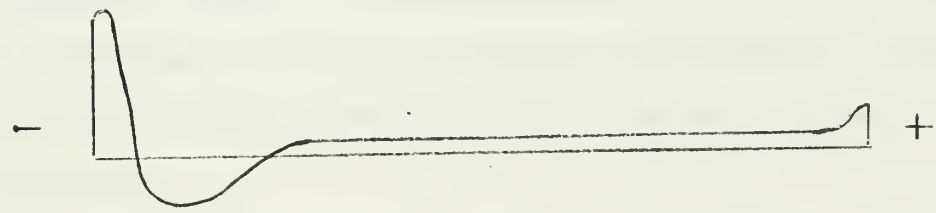

Figure 1d. Field Strength

recent works will be summarized.

Robertson and Hakeem[7] investigated the dependence of striations on the presence of metastable atoms. Moving striations can originate either from instabilities of the plasma, or from oscillations formed at the plasma boundary and propagated through the plasma. Robertson and Hakeem concluded that in both cases, the causes for moving striations are realized only when metastable atoms are present in the glow discharge. If there are no metastable mechanisms available, such as is the case in the alkali glow discharges, then the instabilities are attenuated and moving striations are not observed.

Ascoli-Bartoli, De Angelis and Martellucci[8] used optical interferometry methods to determine electron density distribution in a plasma. Their results are still meager, but the application of Schlieren photography to investigate moving striations may prove to be a very valuable tool in determining the phenomena that accompany them. For example, the analysis of density gradients, if they exist, would lead to information regarding the plasma flow parameters that are associated with the striations.

1.4 Theory

Moving striations travel down thelength of a plasma column with a finite velocity. Cooper[3] has shown that the velocity tends to have several peak values over a range of pressures and currents. The striation velocity is equal to the product of the frequency and wave length of the striations.

If some of the light emitters are moving along the tube with the same velocity as the moving striations, a Doppler shift in the emitted

light should exist. In addition to this source of wave length shift, Doppler broadening and Stark effect cause spectrum perturbations. Doppler broadening is dependent on the random velocity distributions of the emitters within the glow discharge. This results in a smear of spectral lines appearing in place of a narrow, well-resolved single line, The Doppler shift due to the velocity of the moving striations should appear as a well defined shift, and separation of the two Doppler effects is possible provided sufficiently sensitive optical equipments are employed. The Stark effect should not affect the result of this experiment, since it is related to the electric field strength, and in the positive column the electric field strength is low. (See figure 1d.)

If an emitter at rest produces a spectral line of wavelength λ, then it will produce a slightly different wave length λ' when in motion with velocity V.

$$\lambda = \lambda' \left(1 + \frac{v}{c}\right) \tag{1.41}$$

The Doppler shift $\Delta\lambda = \lambda - \lambda'$ that results from velocity V is

$$\Delta\lambda = \left(\frac{v}{c}\right)\lambda' \simeq \left(\frac{v}{c}\right)\lambda \tag{1.42}$$

From this one sees that the velocity is

$$v \simeq c\left(\frac{\Delta\lambda}{\lambda}\right) \tag{1.43}$$

With an anticipated emitter velocity of 90 m/s , one can expect to observe the 8115$\overset{\circ}{A}$ Argon line to shift 2.45×10^{-3} $\overset{\circ}{A}$. In order to detect this magnitude of wave length shift, equipment with a resolving power of $3 \times 10^{+6}$ must be employed.

2. Equipment and Procedures.

2.1 Vacuum System.

A schematic diagram of the vacuum system is shown in figure 2. The system was generally operated at a base pressure of 2×10^{-6} Torr, although it was capable of attaining vacuums in the middle 10^{-7} Torr range. A general photograph of our entire equipment setup is shown in figure 3.

The major components of the vacuum system are one Eimac HV-1 diffusion Pump, one fore pump, two liquid air cold traps, an 80 cm. octoil manometer, a high vacuum Alpert valve, a glass manifold, and two ionization gauges.

The system generally performed in a satisfactory manner; it was a relatively tight system and quite easy to keep clean; however, all operations were greatly slowed down by the Eimac diffusion pump. The operating base pressure of 2×10^{-6} Torr was a compromise between a desired high degree of purity, and the very low pumping rate of the diffusion pump, which was operated with the baffle assembly installed. This mode of operation reduced the pumping speed by a factor of two, but it prevented pump oil from backing up into the rest of the system. Although this type diffusion pump is theoretically capable of attaining a vacuum of 5×10^{-7} Torr, the pumping speed at this pressure is less than 20% of the pumping speed at 2×10^{-6} Torr.

Pump performance was improved by substituting Dow Corning 704 silicone fluid for Eimac Type A diffusion pump fluid. A pressure of 2×10^{-6} Torr could be attained in about five to seven days using the following procedure.

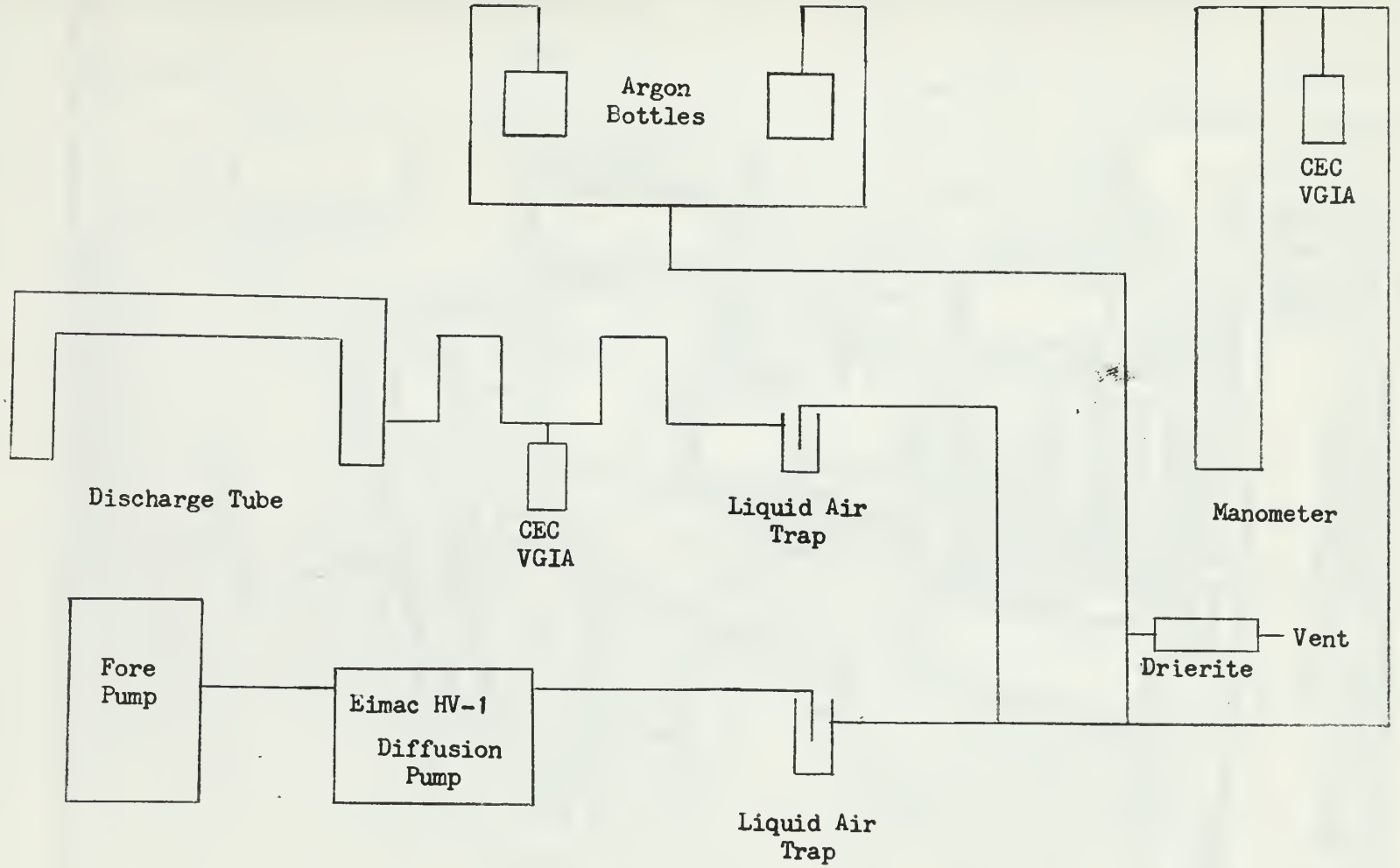

Figure 2 VACUUM SYSTEM SCHEMATIC

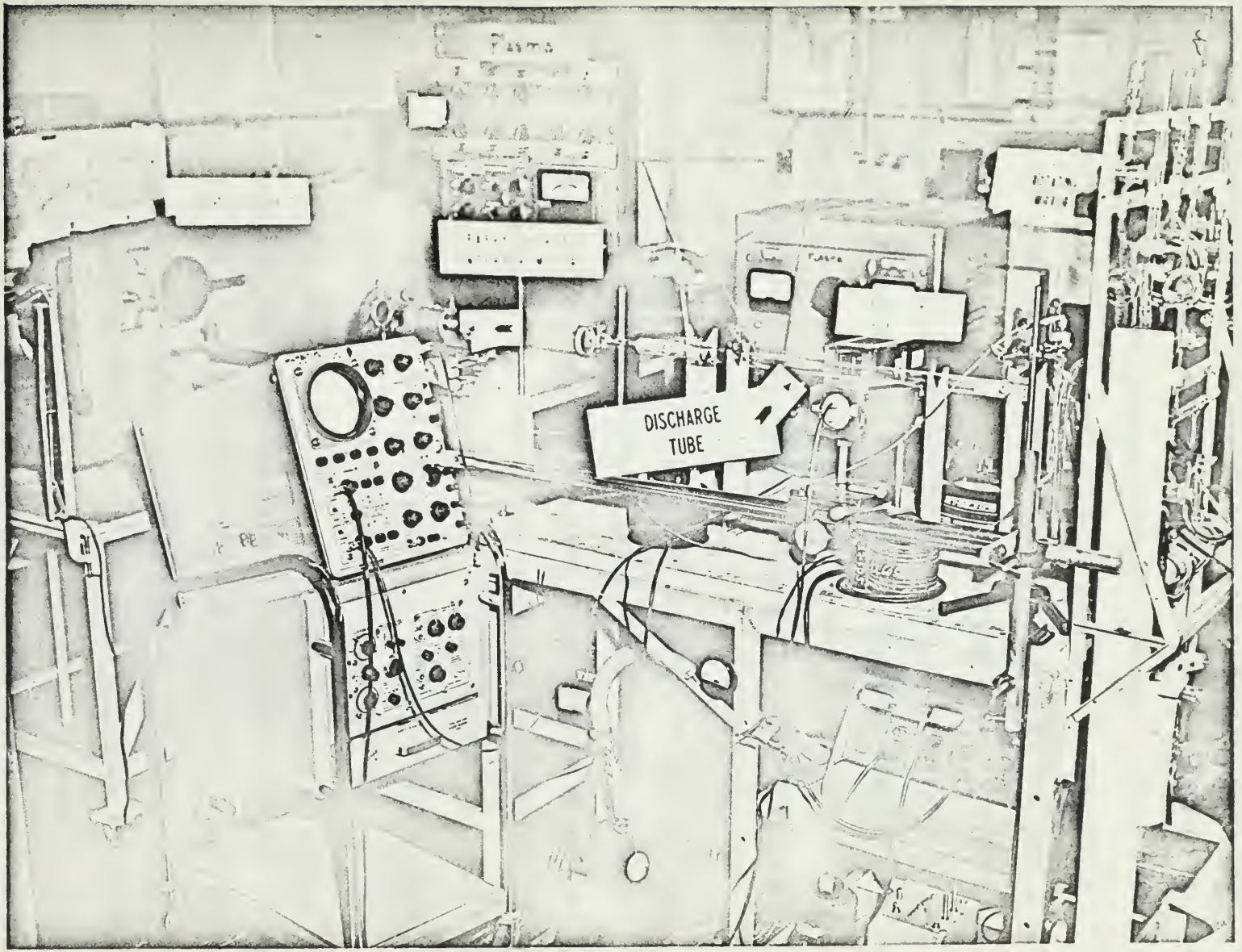

Figure 3. General Equipment Layout

The discharge tube, and portions of the manifold were wrapped with electro-thermal Model H-T 362 heating tapes, initially set at 50 volts. When equilibrium between the pumping rate and the outgassing rate was reached, the voltage on the heating tapes was increased. This was repeated until a maximum voltage of 125 volts was reached. The system was allowed to bake in this configuration for about 24 hours. The electrodes were cleaned by heating to a red-orange color with an induction heater. All filaments were outgassed by heating them with the conventional filament power supply unit. (The power supplies are discussed in more detail in the subsequent section of this paper.) Both of these operations were repeated until equilibrium between the pumping and outgassing rates was established. The heating tapes were operated simultaneously with the electrode heating operation to minimize deposites of outgassed materials being formed on glass portions of the system. Final clean up was attained by operating an Argon discharge, then evacuating the system. This final step was repeated until the Argon discharge attained its characteristic violet glow.

The system's pressure is measured using an ionization gauge VG-1A triode. Argon pressure in the discharge tube was measured using the Octoil S manometer. (One cm. oil equals 0.672 mm. Hg.).

The U-shaped discharge tube was made of Vycor glass. The electrodes were fabricated from Tungsten filament attached to Tantalum supports; circular anodes of Tantalum were similarly mounted. The electrode assemblies were mounted on VG-1A triode bases, which were fused to the discharge tube. This mode of mounting electrodes is very inflexible; cathode replacement is a very inefficient and time consuming process. Discussion

of our experiments with other schemes for mounting the electrodes will be found in section 3 of this paper.

2.2 Electrical System.

The general circuit layout is shown in figure 4. Three power supplies were used. A Kepco, Model 770-B, 600 volt 3 amp. unit provided the high voltage potential for the discharge tube. Fine discharge current control was obtained using a resistor bank.

The filaments were heated with a Kepco, Model KM 236-15A 50 volt, 15 amp. unit. No external control devices were used with this power supply.

A Kepco, Model 500R-B 600 volt, 0.3 amp. unit was used to provide regulated power for the Pupps or auxiliary discharge maintained at the anode end of the discharge tube. A sliding wire resistor was used in this circuit to facilitate current control of the Pupps discharge.

2.3 Electronic System.

Detection of moving striations can be accomplished with a rotating mirror or by electronic methods. We used both systems; the rotating mirror gave us gross information relating to the presence of the moving striations and their stability.

Detailed measurements of various striation parameters such as frequency and wavelength were made using the electronic circuit shown schematically in figure 5. The major components were a Tektronix type 545A oscilloscope, two RCA type 7102 multiplier phototubes, and a battery pack.

The RCA-7102 tube is well-suited for use in the near-infrared region that was of interest to us. Maximum response of the RCA-7120 is the region

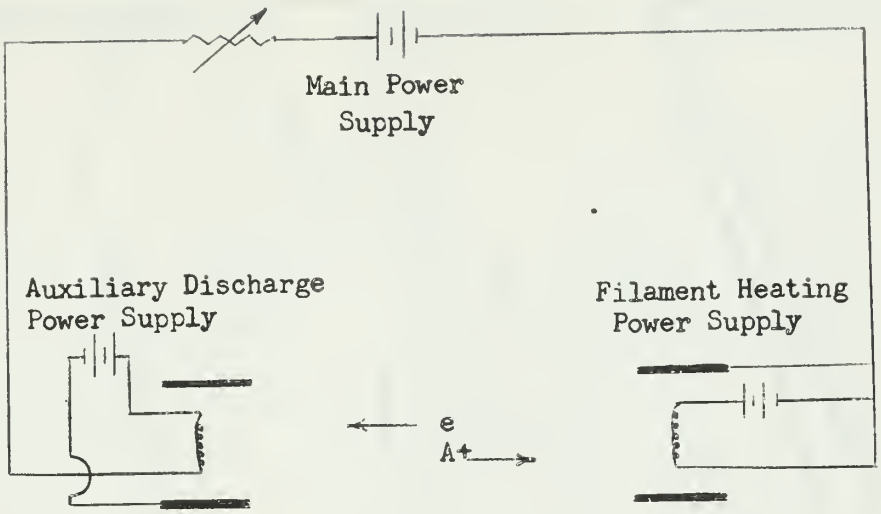

Figure 4. Electrical System

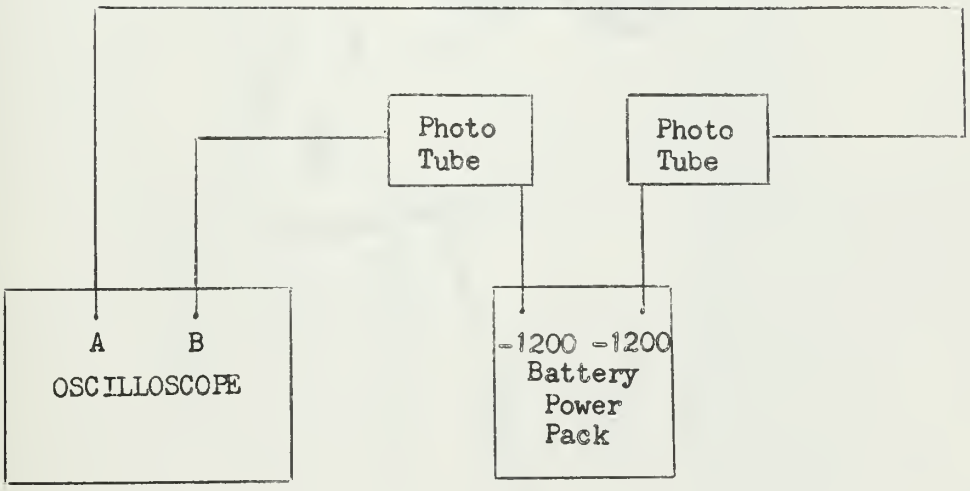

Figure 5. Electronic System

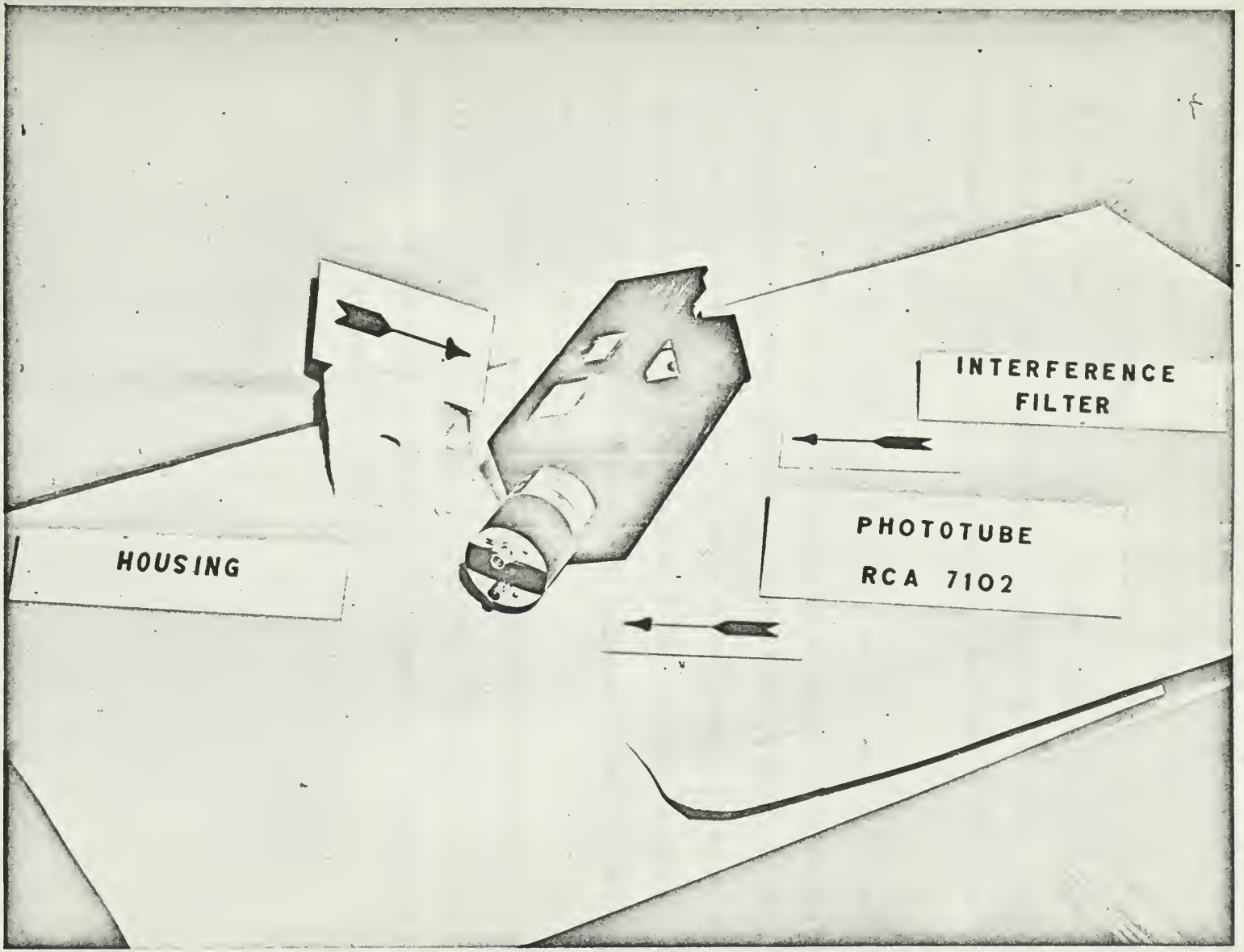

Figure 5. Phototube Assembly

$8000\text{A} \pm 1000\text{A}$, our field of interest fell in this wavelength interval. A battery pack was used to produce a 1200 volt DC source for the photo tubes. Figure 6 shows the method used to mount the tubes.

2.4 Spectrographic Equipment.

In order to be able to measure a Doppler shift in an Argon gas discharge, a Fabry-Perot interferometer was mounted on the optical bench of a Bausch Lomb, Littrow type spectrograph. The general arrangement is shown in figure 7.

The spectrograph's dispersion readily separated the interferometric patterns when entrance slit width was set at 30 microns. Wider entrance slit settings caused overlapping of the Argon lines at 8006A and 8015A. All exposures were made on type I-N Kodak spectrographic plates because of their sensitivity in the 8000A region of the spectrum. A nominal exposure time with this arrangement, an Argon discharge, and a discharge current of 300 ma was three minutes.

The Fabry-Perot interferometer was constructed for maximum resolution in the 7500A to 10,000A region of the spectrum. The details of its construction are contained in Appendix I. The method of calibration and the results are contained in section 5.

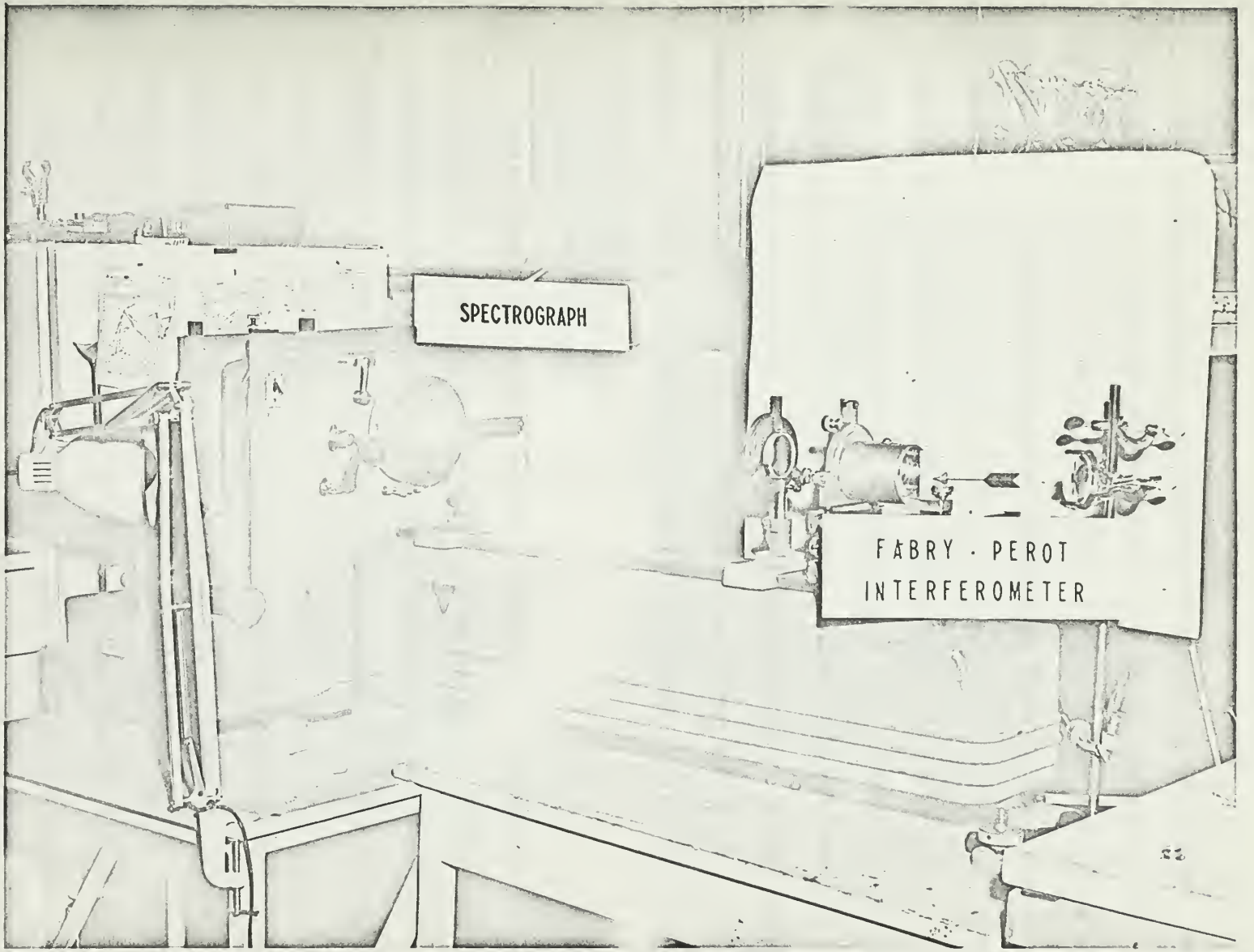

Figure 7. Spectrograph and Interferometer

Feasibility of using a removable end plate tube for gas discharges.

3.1 Problem.

The technique by which gas discharge tubes had been fabricated was reviewed prior to mounting the "U" tube on the vacuum system for the Doppler experiment. Up to this time VGIA ion gauge bases had served as mountings for the electrodes, these bases being fused to pyrex tubing of desired length and diameter to form the closed discharge tube. This technique had distinct disadvantages. For example, the tube had to be completely disassembled when the cathode burned out, a common occurance caused by ion bombardment at high currents. Also different electrode arrangements and materials could not be tried out because of the limited amount of time available. In order to overcome these limitations an attempt was made to establish an argon gas discharge in a tube with removable end plates.

3.2 Procedures and Results.

In an attempt to increase cathode lifetime a "L" dispenser cathode with approximate dimensions of 36 x 36 x 12 mm had been obtained. Previous experiments indicated that an anode configuration as illustrated in figure 8 might induce stability to the amplitude of moving striations as observed on a photomultiplier. As a result of these two considerations, a 40 mm diameter tube was fabricated to an overall length of 92.3 cm using commercial Pyrex O-ring joints and pyrex tubing. In order to silver solder "Hermetic Seal" lead-in pins and facilitate maching, end plates were made of brass. The completely assembled tube is illustrated in figure 9.

The assembly was first tested on a Veeco vacuum leak detector. The tube was evacuated to the 10^{-5} Torr range in about ten minutes. Spraying the exterior of the end plates and seals with helium indicated neg-

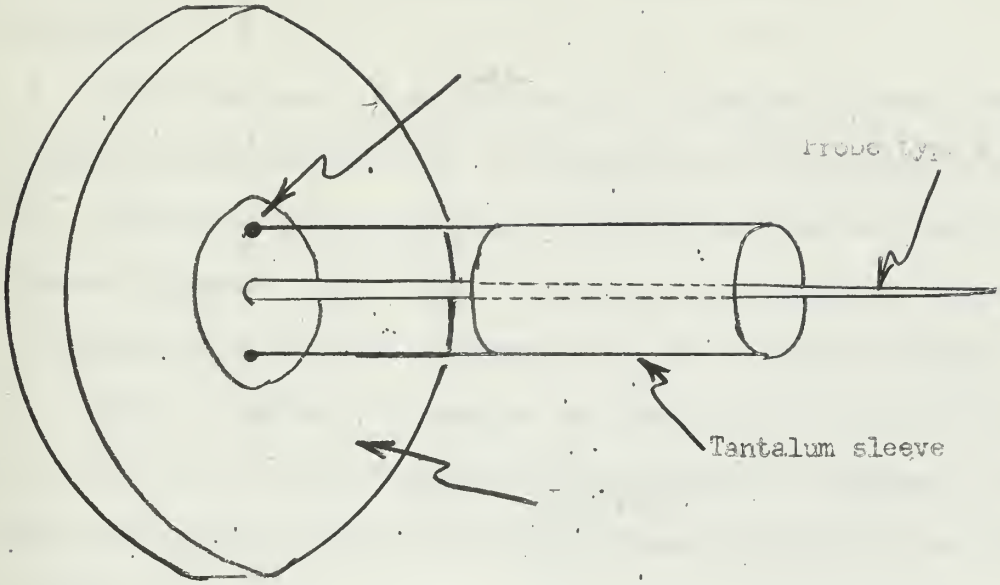

Figure 8. Anode Configuration

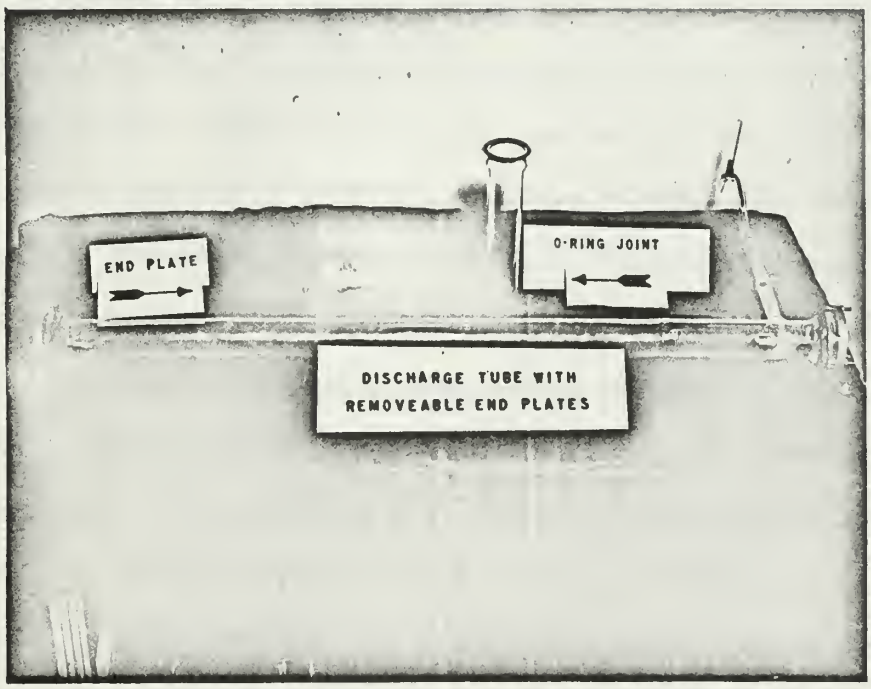

Figure 9. Removable Endplate Assembly

ligible leakage. The tube was then fused to the vacuum system, evacuated, and baked out with heating tapes. A base pressure of 5×10^{-6} Torr was obtained.

An attempt was made to activate the dispenser cathode; however, this attempt failed primarily due to inexperience with activation procedures (i.e. decomposition of strontium carbonates was too fast due to excessive filament temperature). A helical wound tungsten filament with a cylindrical shield was substituted for the dispenser cathode.

With the system re-evacuated and baked out to a base pressure of 2×10^{-5} Torr, the tube was filled with argon to a pressure of 5 mm Hg. When a discharge could not be obtained using a 600 volt power supply, a 1200 volt, 0.75 ma, DC power supply was placed across the tube. A discharge was obtained with this power supply; however, after about a minute of operating a break-down occurred between the electrode and the end plate at the cathode which exceeded the current capacity of the power supply. The end plates were removed and the anode plate was coated by brush with glyptol insulating varnish and the cathode plate with a dissolved lucite dope. The tube was reactivated; however, the lowest obtainable base pressure was 3×10^{-5} Torr. The tube was filled with argon, but on this occasion the discharge became unstable and extinguished itself with a change of color that indicated possible contamination. It is believed that leakage was occuring around the "O" rings due to the rough nature of the dielectric coatings. At this point, because of time limitations, the removable end plate investigation was discontinued and VGIA bases were used to assemble electrodes with thoriated tungsten filaments. These bases were then fused onto the "U" tube.

Using a center intense image the spacer may be ground and adjusted with spring tension to parallelism within about a hundredth of a wavelength of the reference light. Thus any further changes of the fringe pattern as the eye is moved across the field would be due to lack of optical flatness of the plates.

When the spacer was ground as exactly as possible the aluminized plates were removed and the dielectric coated plates were substituted in their place. The interferometer was set up an the optical bench of a Bausch and Lomb Littrow type spectrograph.

The interferometer was adjusted using a Neon Geissler tube and ground glass diffuser as a light source. Sufficient red light in the visible spectrum was reflected by the dielectric coating so as to be produce a weak interference pattern. The eye when focused at infinity could distinguish this pattern against the background intensity sufficiently well to allow adjustment of the interferometer springs for parallism.

Next a white light source was placed at the plate holder of the spectrograph in order to project the optical axis from the entrance slit of the spectrograph. The focusing lens was positioned by autocollimation using this source and the image of the spectrograph slit projected onto itself.

The next problem incurred was that of placing to interferometer on its table such that the vertical diameter of interference pattern was coincident with the slit of the spectograph. Reflectance of the interferometer plates in the visible region was insufficient to allow projection of the interferometric pattern onto the entrance slit.

Although the removable end plate tube did become operational, it is felt that this method of assembly is practical.

3.3 Conclusions

It is recommended that the following steps be taken. (1) A 25 mm tube be assembled of 90 cm length in order to reduce the current in the discharge. (2) End plates be made of $\frac{1}{2}$" or 3/4 phenolic insulating board rather than brass. (3) Lead-in seals be set in with vacuum epoxy using 4 parts 828 epoxy resin and 1 part Shell Epon curing agent "U".

4. Investigation into Two Methods for Obtaining Radial Distribution of Emitters from Spectroscopic Measurements.

4.1 Problem.

It is possible to investigate certain parameters of optically-thin plasmas using spectroscopic techniques. These methods leave the plasma virtually undisturbed; however, the data are frequently very difficult to interpret. Barr[9] and Bockasten[10] have reported on methods to convert observed radiation intensity profiles from an optically thin cylindrical source into an expression for the radial distribution of emitters. Basically, both methods are readily adaptable to computer programs for the Control Data Corporation Model 1604 Computer at USNPS.

From the nature of the mathematical transformations that were used in the development of both systems, there appears some question regarding the sensitivity of the observed intensities to small changes in the radial distribution. There was also a need for curves of expected intensities from assumed radial distribution. These two questions could be answered simultaneously, with the results yielding some insight into the relative accuracy of each method.

4.2 Procedure.

A highly colimated detector mounted as shown in figure 10, accepts th energy from a very narrow tube of light through the source.

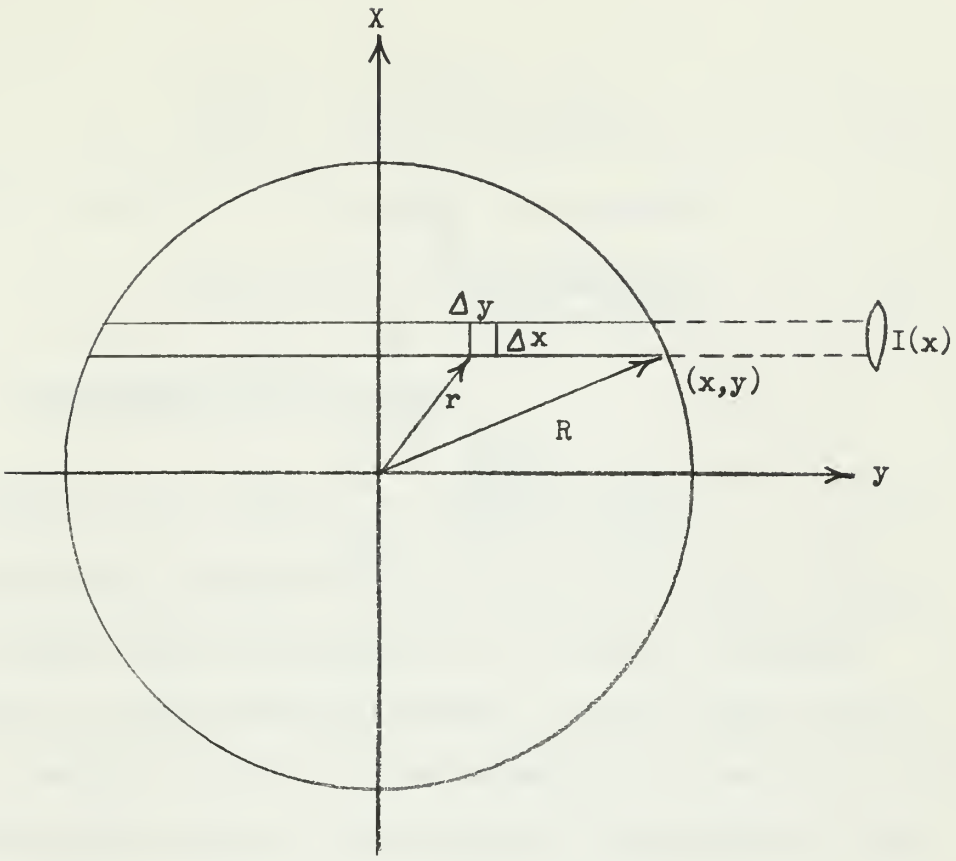

Figure 10

Plasma Disk showing coordinate system

(The Z axis is directed into the paper)

The radial distribution of emitters, E(r), is assumed to be circularly symmetric with respect to the Z axis; the radiation is assumed to be isotropic, and not absorbed by the plasma. Under these conditions,

$$I(x)\,\Delta x \Delta z = 2\sum_{y=0}^{y_0} E(r)\;\Delta x\,\Delta y \qquad (4.1)$$

Expression (4.1) reduces to the integral equation (4.2) when infinitely small volume elements are considered.

$$I(x) = 2\int_{o}^{y_o} E(r)\,dy \tag{4.2}$$

Using the fact that $y^2 = r^2 - x^2$, equation (4.2) becomes:

$$I(x) = 2\int_{x}^{R} \frac{E(r)\,r\,dr}{(x^2-r^2)^{1/2}} \tag{4.3}$$

Using Abel's transformation /11/ this becomes:

$$E(r) = -\frac{1}{\pi}\int_{r}^{R} \frac{\frac{dI(x)}{dx}\,dx}{(x^2-r^2)^{1/2}} \tag{4.4}$$

The observations that yield I(x) in practice do not give a smooth curve or an easily plotted function, but only a series of numerical values. There are various numerical methods to convert these empirical values into a smooth curve, I(x). Since equation (4.4) uses the derivative of I(x). This system possesses certain inherent insensitivities which must be investigated.

Equation (4.3) can be used to evaluate expected observed intensities from assumed radial distributions. On can evaluate I(x) exactly from a well behaved function such as $E(r) = 1 - (\Delta\, r_j)^2$; however, such simple functions are too few in number to be of much help; therefore numerical methods must be used.

A relatively simple expression for I(x) can be obtained by fitting E(r) to a second degree polynominal in the same manner as Barr /9/.

$$I(x_k) = \Delta \sum_{j=k}^{20} a_{jk}\, E(r_j) \tag{4.5}$$

where Δ equals .05 and the coefficients A_{jk} are determined according to (4.6).

$$a_{jk} = 4/3\,(2k+1)^{1/2} \quad \text{if } j = k$$

$$a_{jk} = \left\{ \frac{[(j+1)^2-k^2]^{3/2}}{(2j+1)} - \frac{4j(j^2-k^2)^{3/2}}{4j^2-1} + \frac{[(j-1)^2-k^2]^{3/2}}{2j-1} \right\} \quad (4.6)$$

if $j \neq k$

A comparison between the values of I(x) for $E(r) = 1-(\Delta^r_j)^2$ obtained from equations (4.3) and (4.5) is shown in figure 11. Figures 12, 13, and 14 show expected I(x) curves determined by equation (4.5) from 15 assumed radial distributions. In all graphs, both E(r) and I(x) are normalized so that their maximum values are equal to unity. All transformations are based on 20 equal increments ( ), with E(r) reducing to zero at the outer boundary of the plasma, both I(x) and E(r) having zero slopes at the origin. The numerical values used to plot figures 12, 13, and 14 are tabulated in table 2 of Appendix II.

We did not have a satisfactory discharge tube for making intensity observations to compare the Barr and Bockasten methods. Therefore the 15 sets of calculated values for I(x) were used as inputs to determine the corresponding radial distribution using both methods. The computed values are tabulated in table 3 of Appendix II.

4.3 Results and Conclusions.

The errors inherent to the numerical methods employed in equation 4.5 do not appear excessive. The maximum error shown figure 11 is 1.5%, but the average value at each calculated point is 0.1761%. Therefore, we assumed that the numerical methods used in converting the assumed radial densities into profiles are at least as accurate as the experimental measurements.

The 15 radial distributions were not selected randomly, but with three objectives. First, some were used because they closely approximated

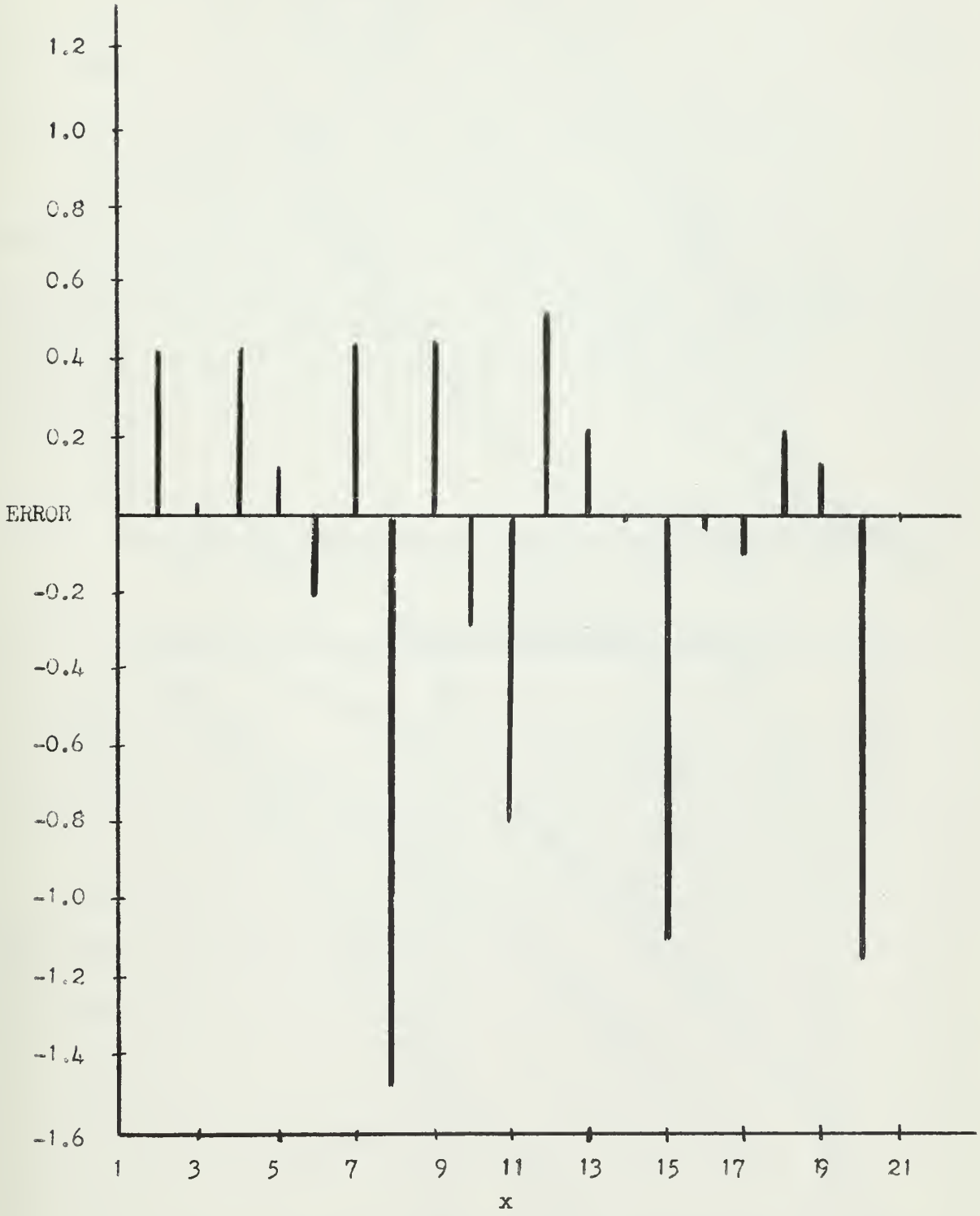
COMPARISON BETWEEN EXACT
AND
NUMERICAL METHOD SOLUTIONS
1.2
1.0
0.8
0.6
0.4
0.2
ERROR
-0.2
-0.4
-0.6
-0.8
-1.0
-1.2
-1.4
-1.6
1
3
5
7
9
11
13
15
17
19
21
x

Figure 11

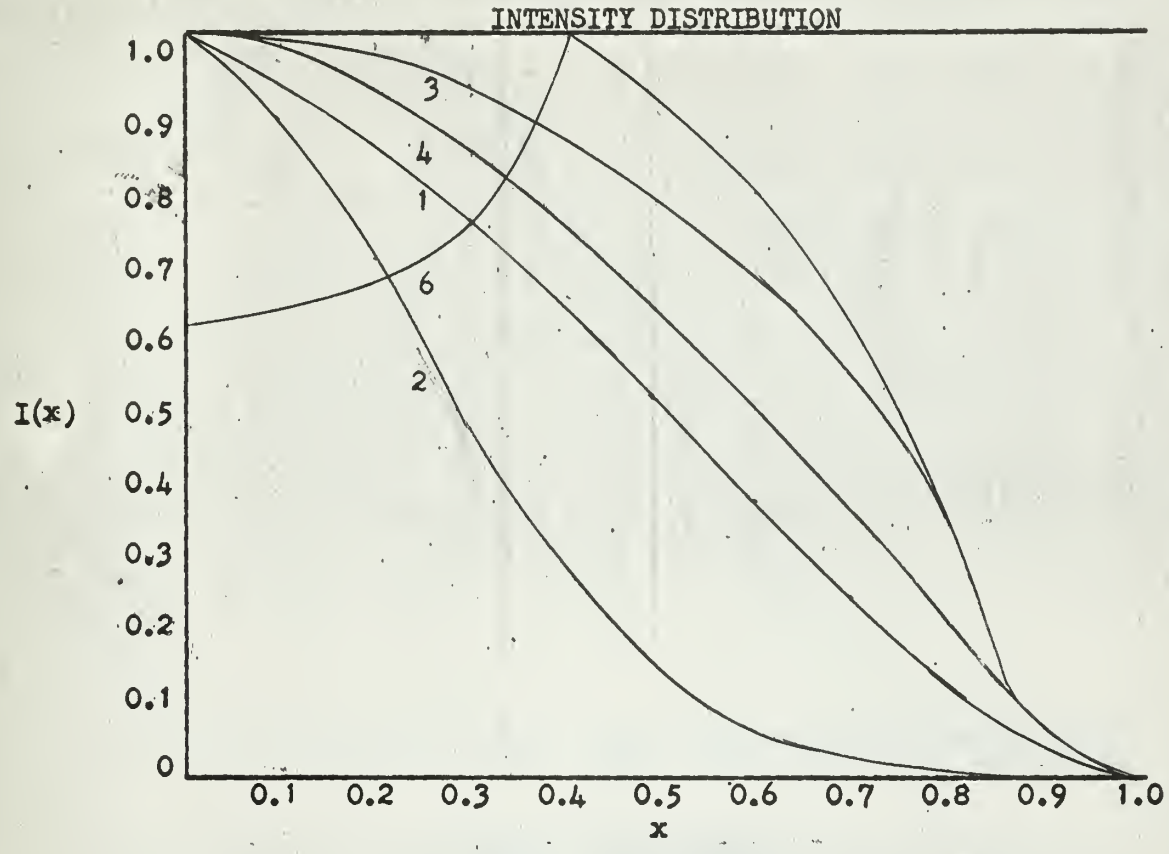
INTENSITY DISTRIBUTION
I(x)
1.0
0.9
0.8
0.7
0.6
0.5
0.4
0.3
0.2
0.1
0
0.1 0.2 0.3 0.4 0.5 0.6 0.7 0.8 0.9 1.0
x
3
4
1
6
2

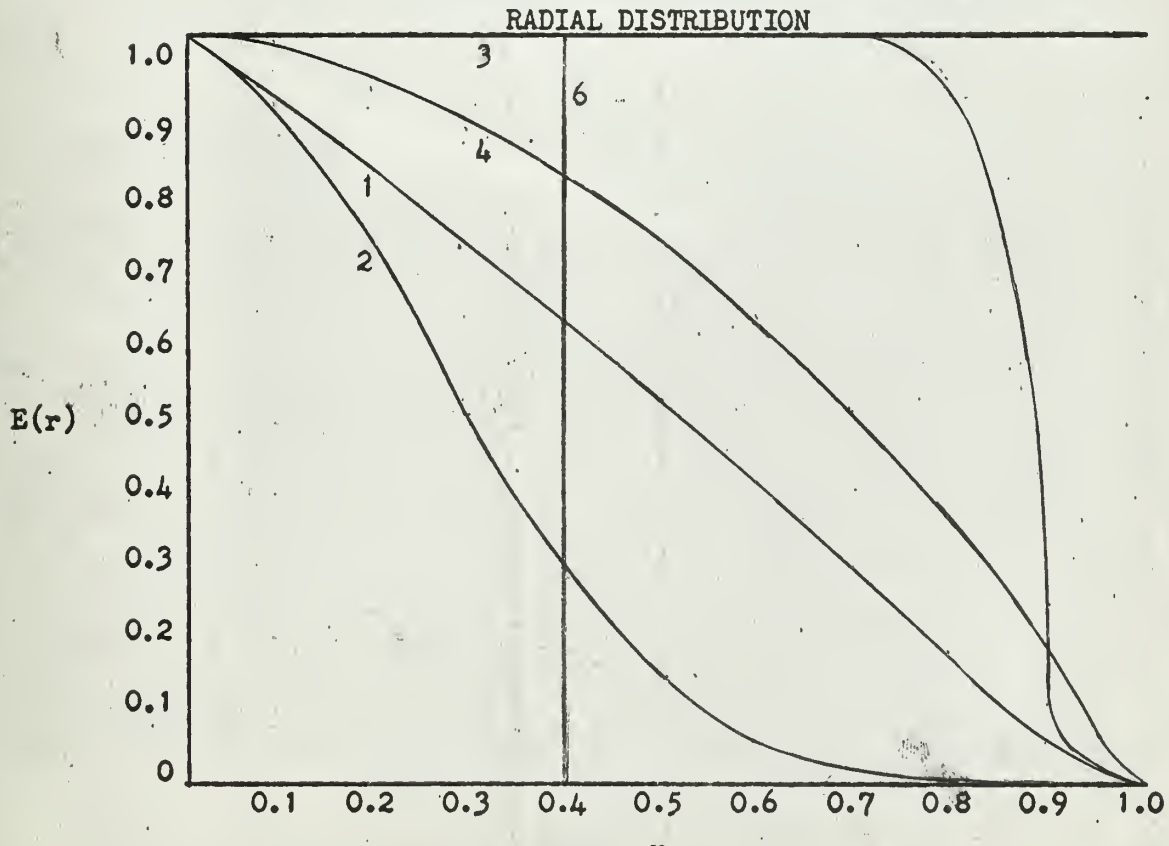
RADIAL DISTRIBUTION
E(r)
1.0
0.9
0.8
0.7
0.6
0.5
0.4
0.3
0.2
0.1
0
0.1 0.2 0.3 0.4 0.5 0.6 0.7 0.8 0.9 1.0
r
3
6
4
1
2

Figure 12

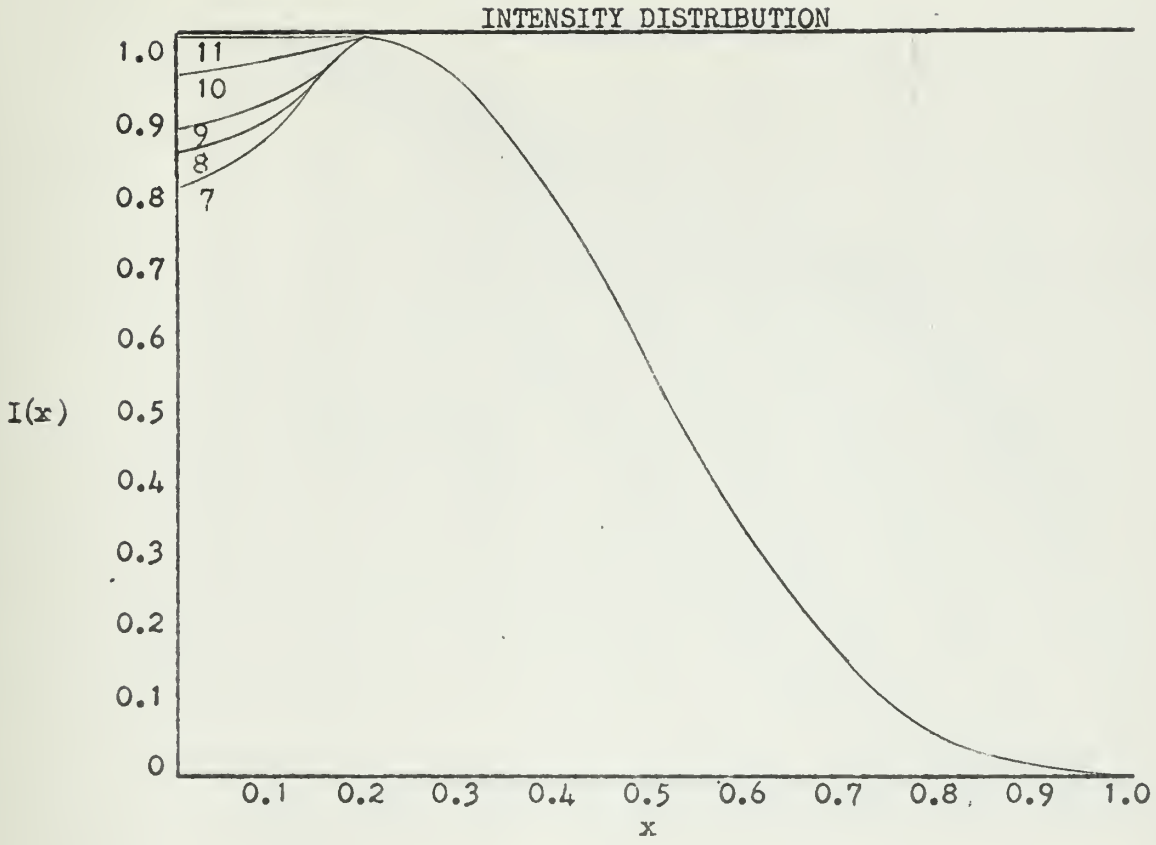
INTENSITY DISTRIBUTION
I(x)
1.0
0.9
0.8
0.7
0.6
0.5
0.4
0.3
0.2
0.1
0
11
10
9
8
7
0.1
0.2
0.3
0.4
0.5
0.6
0.7
0.8
0.9
1.0
x

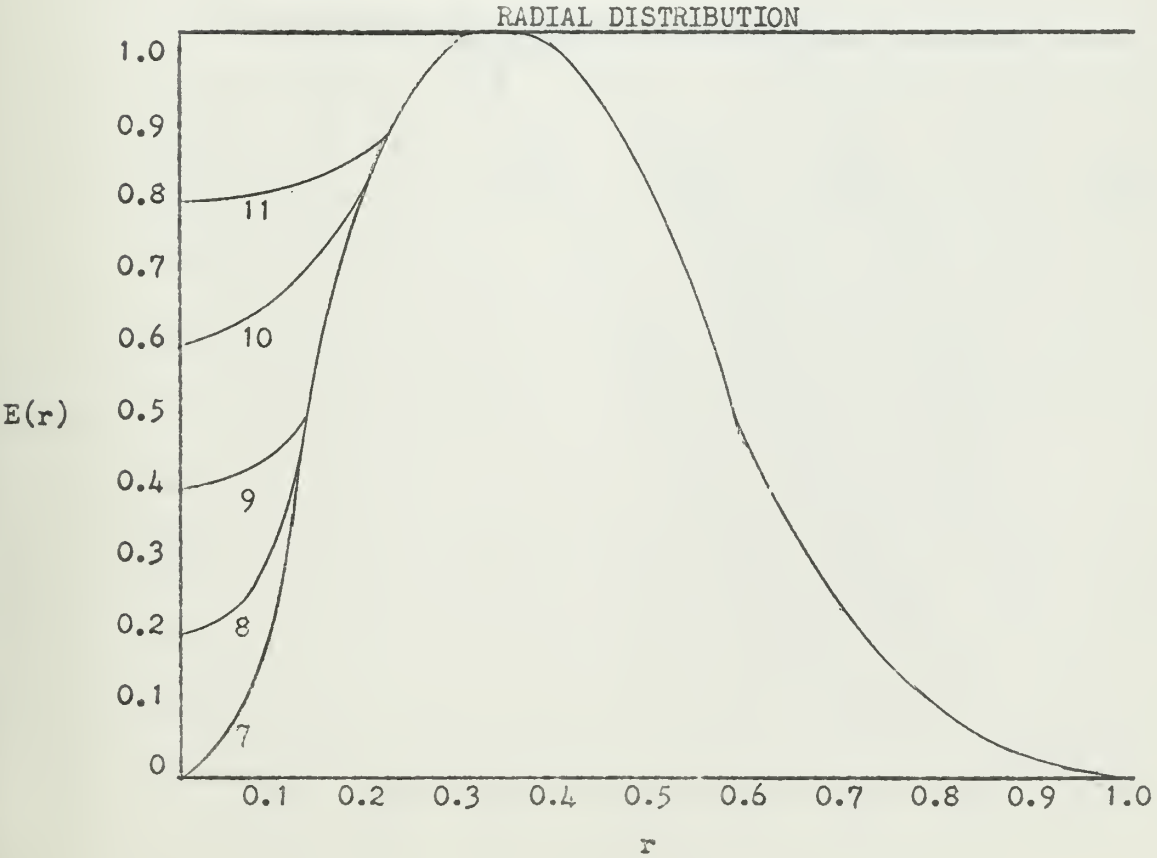
RADIAL DISTRIBUTION
E(r)
1.0
0.9
0.8
0.7
0.6
0.5
0.4
0.3
0.2
0.1
0
11
10
9
8
7
0.1
0.2
0.3
0.4
0.5
0.6
0.7
0.8
0.9
1.0
r

Figure 13

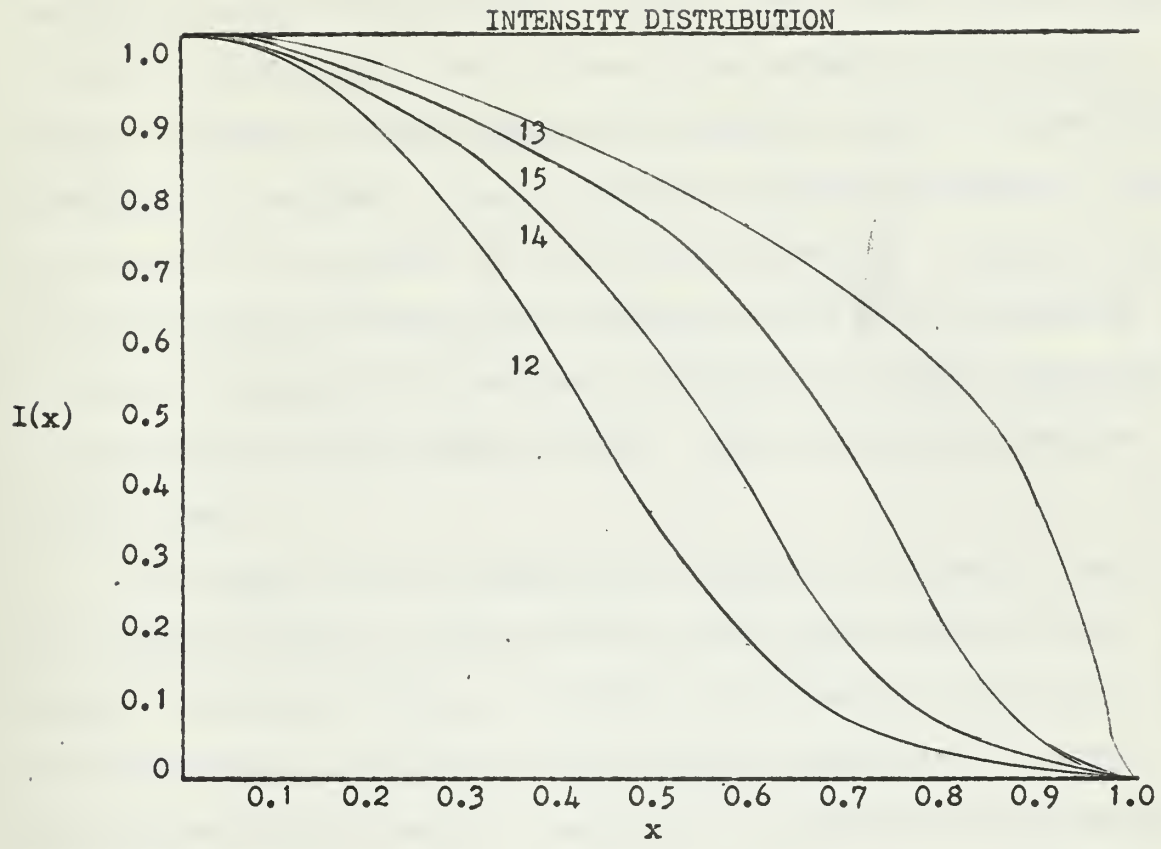
INTENSITY DISTRIBUTION
I(x)
1.0
0.9
0.8
0.7
0.6
0.5
0.4
0.3
0.2
0.1
0
13
15
14
12
0.1 0.2 0.3 0.4 0.5 0.6 0.7 0.8 0.9 1.0
x

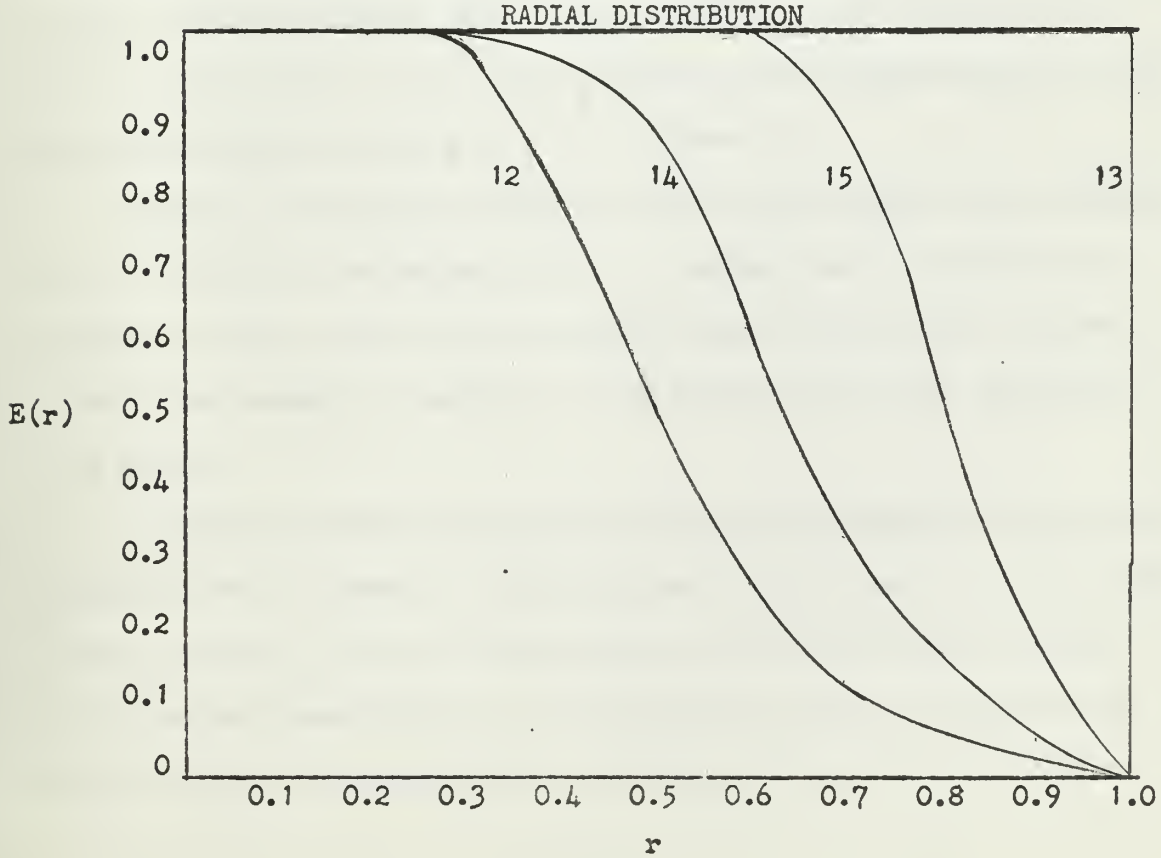
RADIAL DISTRIBUTION
E(r)
1.0
0.9
0.8
0.7
0.6
0.5
0.4
0.3
0.2
0.1
0
12
14
15
13
0.1 0.2 0.3 0.4 0.5 0.6 0.7 0.8 0.9 1.0
r

Figure 14

physically measured distributions. The zero order Bessel function (curve 1) and the Gaussian distribution (curve 2) are examples of this type. Second, families of similar curves were selected in order to determine the sensitivity of intensity curves to changes in radial distribution. Curves 7-11 and 12-15 are examples of this method of selection. Finally, some "limiting value" distributions were selected. They are not physically possible, but their discontinuities do represent the boundary conditions within which all distributions must lie. Curves 6 and 13 are examples of this type.

It is apparent from an inspection of figures 12, 13, and 14 that the observed intensity profile does not change nearly as much as the radial distribution function. Note that in the family of curves 7-11, E(0) varies from 0 to 0.8, but I(0) varies only from 0.8 to 1.0. One may conclude that the density of emitters at the center of the cylinder is not a maximum value if the intensity profile is not maximized at $x = 0$. The converse is not true, I(0) may be the maximum value of I(x), and a rarefaction may occur at $r = o$. (curve 11).

A general, qualitative picture of the radial density may be obtained by curve fitting an experimental plot of intensities to those curves obtained in this paper from the assumed radial distributions; however, quantitative values of electron or atom density can not be obtained by this method.

A comparison between the methods of Barr and Bockasten using these assumed curves is somewhat artificial, since the curves are not all physically possible, and the discontinuities strain both methods beyond their designed capabilities. An inspection of table 3 of Appendix II shows that neither method is very reliable near the outer boundary of

the region containing the emitters. Generally, the errors produced by the Barr method are larger than those produced by Bockasten's method by a factor of at least two. The errors in both cases change sign frequently, indicating an oscillation or crossing of the exact curve by the generated curve.

Barr's method incorporates a least squares correction to improve the quality of input data. This causes an anticipation of large changes in radial distributions, and hence a rounding off of the generated intensity curves. Consequently Barr's errors are larger on a point-by-point comparison, but the overall curves are just as valid as Bockasten's curves.

The inversion of the $I(x)$, profiles can give, at least, only relative values of the radial variation of the emitters, $E(r)$. The interpretation of the radial density of emitters in terms of the radial variation of electron density, for instance, requires certain assumptions about the uniformity of temperature, density of atoms, etc. The magnitude of the electron density must be obtained by some other method, such as measurements of absolute intensity.

5. Doppler Shift Experiment

5.1 Problem.

The problem for which this experiment was designed is discussed in Section 1.4. To review briefly, a Doppler shift should exist if the phenomena of moving striations in gas discharges is due to the collective motion of the light sources. Therefore, the objective was to make a measurement of sufficient precision to determine if such a Doppler shift occurs.

The experimental lay-out consisted of a "U" shaped gas discharge tube with windows at the base which provide a means to view the positive column. On a line with this section of the discharge was the optical bench of a spectrograph upon which was mounted the necessary focusing lens and a Fabry-Perot interferometer. A shift in the interferometric pattern when the striations were moving in one direction versus moving in the other direction would indicate the Doppler shift.

5.2 Instrumentation Parameters.

The initial parameters for the experiment were established in the following manner. From the work of A. W. COOPER it appeared feasible to obtain moving striations in a gas discharge in Argon with a velocity of 90 meter/sec. By comparing striations moving toward to those moving away from the interferometer a difference of velocity of 180 m/sec. could be obtained. As previously mentioned, the work of Robertson and Hakeem established the dependence of striations on the metastable state. Accordingly as part of the experimental procedure the wave lengths in Argon upon which the measurement would be attempted would include decays to the metastable states. In Argon such wavelengths are in the near red region

of the spectrum. The expected doppler shift would be:

$$\Delta\lambda = \left(\frac{v}{c}\right)\lambda = 8115\text{Å}\left(\frac{1.8\times10^{2}}{3\times10^{8}}\right) = 0.005\text{Å}$$

For a Fabry-Perot interferometer the intensity, I, at any point in the field is the following function of I_o, the uniform monochromatic source intensity,

$$I = I_o\left(\frac{1}{1 + a^2 \sin^2 d/2}\right) \tag{5.1}$$

where $a^2 = \frac{4R}{(1-R)^2}$

$$d = 2\pi\left(\frac{2t\mu}{\lambda}\cos\theta\right)$$

R is the reflectance of the plates, t is the thickness of the spacer, μ is the index of refraction of the gas in the space between the plates, λ is the wave length of light. The half width of an interference fringe is given by quanity $a \sin d/2 = \pm 1$. For a high resolution instrument this value may be obtained as a small perturbation of an order of interference.

$$d = 2\pi(n+\varepsilon) \tag{5.2}$$

Where n is an integer, ε is a perturbation

$$\sin d/2 = \sin\pi n \cos\pi\varepsilon + \cos\pi n \sin\pi\varepsilon$$

$$\simeq \pi\varepsilon \quad \text{for} \quad \varepsilon \text{ sufficiently small}$$

Therefore

$$a\pi\varepsilon \simeq \pm 1 \tag{5.3}$$

But, by taking the differential of the argument

$$\varepsilon = d\left(\frac{2t\mu\cos\theta}{\lambda}\right) = \frac{-2t\mu\cos\theta\, d\lambda}{\lambda^2} \tag{5.4}$$

$$\varepsilon = -n\frac{d\lambda}{\lambda}$$

Substituting 5.3 into 5.4.

$$\Delta\lambda = \frac{\varepsilon\lambda}{n} = \frac{\lambda^2}{2t\mu\pi a}$$

Assuming that the index of refraction is unity, that plates have 99% reflectance and a wavelength of interest is 8115Å the minimum spacer thickness for measuring a 0.005Å shift is:

$$t = \frac{\lambda^2}{2\pi a\,\Delta\lambda} = \frac{(8115\,\text{Å})}{(2\pi)(200)(0.005\text{Å})} \simeq 1\ \text{MM}$$

In order that spacer thickness would not be the limit of resolution the latter was made approximately a order of magnitude larger than the calculated minimum.

The instrumental broadening caused by lack of flatness of the plates can be calculated to a first approximation. The dielectric plates were specified flat to within 1/100 of a wave length of a Hg green line. The resulting change in order of interference δm of the plates due to lack of flatness δt is: $m\lambda = 2t$

$$\delta m\,\lambda = 2\,\delta t$$

$$\delta m = \frac{2}{\lambda}\left(\frac{\lambda_o}{100}\right) \qquad (5.5)$$

where λ_o is wavelength of Hg green line. The expected change of the order of interference due to Doppler shift Δm is:

$$\frac{\Delta m}{m} = \frac{\Delta\lambda}{\lambda} \qquad (5.6)$$

Thus, the ratio of the changes in order is:

$$\frac{\delta m}{\Delta m} = \frac{2}{m\,\Delta\lambda}\left(\frac{\lambda_o}{100}\right) = \left(\frac{\lambda_o}{100}\right)\frac{c}{t\,v} = \frac{5600\text{Å}}{100}\left(\frac{3\times10^8\ m/sec}{1cm\times180\ m/sec}\right) = 0.8 \qquad (5.7)$$

For a one centimeter spacer, the change of order of interference due to irregularities in the flatness of the plates amounted to approximately eight tenths the order of interference change due to Doppler shift. Thus, the expected instrumental broadening was 0.004A. Obviously this condition placed a lower limit on practical spacer size.

Dielectric coated plates with the specified flatness were obtained from Perkin Elmer Corp. and a 8.679 ± 0.001 mm spacer was manufactured of Invar. The interferometer was assembled as described in Appendix I.

5.3 Interferometer Calibration.

Zeeman splitting of Argon was used to determine the minimum resolution of the Fabry-Perot interferometer. An Argon Geissler tube was located normal to the axis of a six inch circular pole piece, $2\frac{1}{2}$-inch gap electromagnet. The magnet provided cross fields of up to three kilo gauss. An image of the source was focused onto the optical axis of the interferometer and spectrograph. Exposures were taken at various values of magnetic field strength. Line traces were then made on the interferometric pattern using a Knorr-Alber microphotometer. With a 25mm slit height only two interference fringes were imaged on the photographic plate. Expected Zeeman spitting patterns for lines in the region of interest are shown in figure 15. These patterns were calculated for a nominal field strength of 10,000 gauss.[12] Several line patterns were analyzed and the best resolution was obtained on argon 8015Å where the splitting could be observed at 300 gauss. This corresponds to a wavelength shift of 0.015Å, a factor of three larger than the desired resolution.

Certain problems became apparent while making the calibration plates. First, line widths were approximately 0.03Å. It was not determined at

ZEEMAN SPLITING IN ARGON

B Field = 10^4 gauss

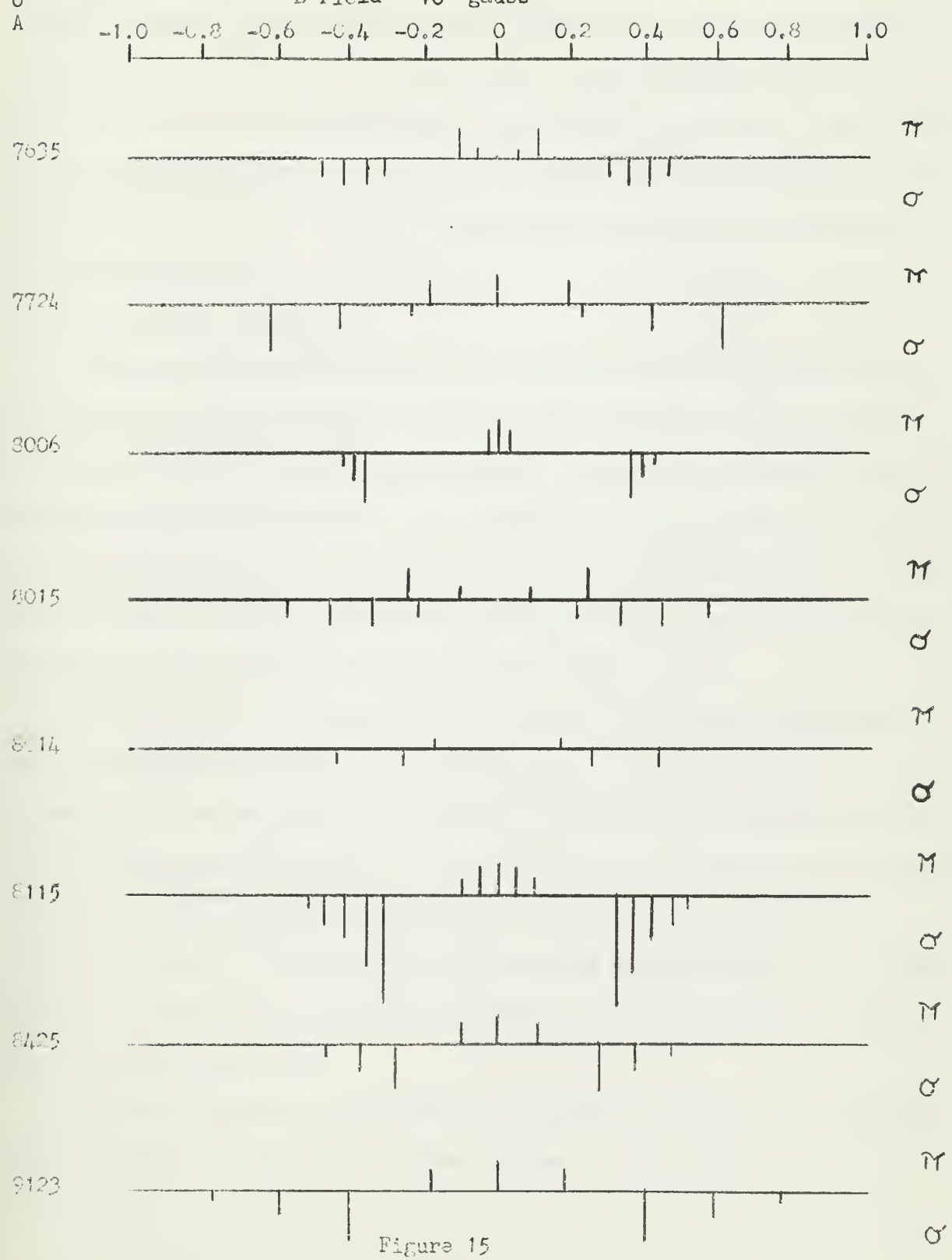

Figure 15

this point whether the lines were instrumental broadened or source broadened. Second, it was necessary to stop the microphotometer down to a small aperture, approximatley 0.5mm x 0.05mm in order separate adjacent lines. To compensate for the small aperture the sensitivity of the instrument was raised to the maximum value. As a result the emulsion "noise" level showed significantly on the line trace. The results of the calibration runs indicate that at least a factor of three must be gained in the resolution of the interferometer.

5.4 Results and conclusions.

An attempt was made to complete the experiment; however, other factors degraded the results. Several casualties were sustained in the discharge tube while trying to conduct the experiment. On only one occassion was the experiment completed satisfactorily. However, on that occassion the striation velocity was 26 m/sec, a factor of four below the desired 90 m/sec. A velocity as high as 52 m/sec, was obtained during one of the unsuccessful runs. No Doppler shift could be detected in the 26 m/sec. run.

An overall factor of eight must be gained in the system performance before satisfactory results may be anticipated. In order to obtain this improvement, the answer must be determined as to whether the broad line width of the interferometric patterns is caused by source broadening or instrumental broadening. The interferometer should be checked against a narrow line width source such as a Schuler tube to make this determination. If the broad width is caused by the source, the interferometer resolution may be improved by increasing spacer size.

Even with improved interferometer resolution, the measurement of small Doppler shifts on broad lines imposes problems. These might be

solved by using a narrow line width absorbsion cell in the optical path or by using $\frac{1}{4}$ power points of off center images in the Fabry-Perot field. This latter method consists of adjusting the interferometer so that the line of interest just appears as a first interference ring. The "tail" of the line intersects the axis of the interferometer at the $\frac{1}{4}$ power point as shown in figure 16. The height of the center portion of the pattern would then be a very sensitive measurement of the broadness of the line and would reflect a Doppler shift should it exist.

An increase of signal to noise ratio on the microphotometer traces is another improvement which must be made in either case. This might be obtained by using an emulsion with fine grain, such a type IV plate .

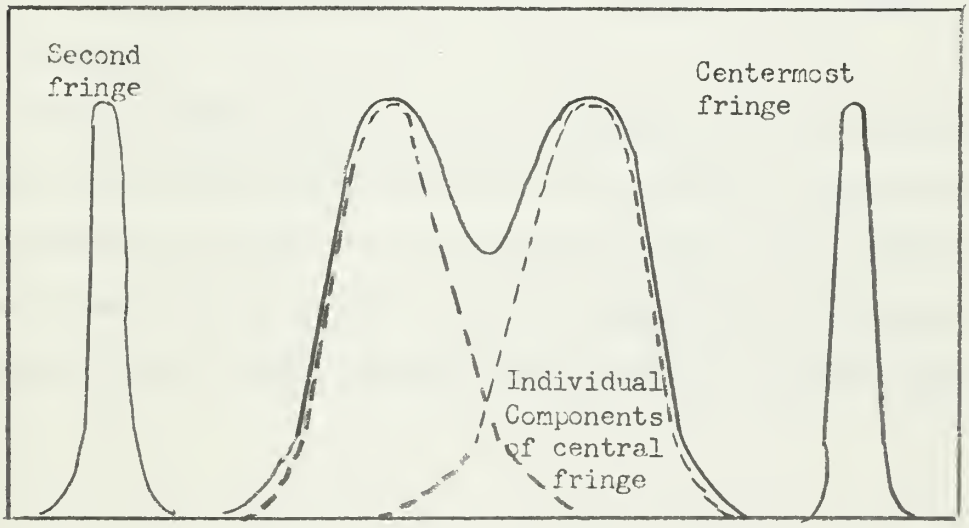

Figure 16

Quarter Power Point Resolution of Fabry-Perot Interferometer

6. Recommendations

It is recommended that the following areas be investigated by future research groups at USNPGS. These recommendations are based upon problems we encountered and subjects of interest that became apparent during the course of our experimenting.

The removable endplate concept should be reviewed, and investigation made into locating an endplate material that would perform satisfactorily as an insulator and maintain a vacuum of 10^{-7} Torr.

Experiments should be made to compare the spectroscopic method of obtaining emitter distribution with probe and/or microwave techniques. Spectroscopic data should be reduced by both the Barr and Beckasten methods in order to gain further insight regarding the relative merits of each method

Further attempts should be made to determine if an orderly motion of atoms occurs when moving striations are observed in a glow discharge. The discharge tube used for this experiment should have a smaller inside diameter than the tube we used, because a smaller tube will produce moving striations with a greater velocity, thus producing a greater Doppler effect.

7. Acknowledgements

The authors wish to acknowledge the assistance of Professor R. L. Kelly for his counsel and advice, and Professor A. W. Cooper for his aid in maintenance of the vacuum system. We are also indebted to Professor J. H. Duffin for his assistance in preparing the computer programs.

We also gratefully acknowledge the technical assistance of Messers L. Smith, R. C. Moeller, and J. Calder.

Bibliography

1. Sanborn C. Brown, Speech, Sigma Xi - RESA National lecture, 1960

2. J. J. Thompson and G. P. Thompson, Conduction of Electricity Through Gases, (Cambridge University Press, 1933) 3rd. Ed., Vol II.

3. A. W. Cooper, Moving Striations in the Inert Gases, (Ph.D. Thesis, Queens University of Belfast, 1961)

4. Sanborn C. Brown, Basic Data of Plasma Physics, (The Technology Press and Wiley and Sons, Inc., New York, 1959), Chap. 14.

5. F. H. H. Kinley and R. J. O'Malia, A Spectroscopic Investigation of An Argon Glow Discharge, (M. S. Thesis, U. S. Naval Postgraduate School, 1962).

6. Gorden Francis, The Glow Discharge at Low Pressure. (Handbuch der Physik, Springer - Verlag, 1956), Vol XXII.

7. H. S. Robertson and M. A. Hakeem, Proceedings of the Fifth International Conference on Ionization Phenomena in Gases, (North Holland Publishing Company, Amsterdam, 1962) p. 550.

8. U. Ascoli - Bartoli, A. De Angelis, and S. Martellucci, Proceedings of the Fifth International Conference on Ionization Phenomena in Gases, (North - Holland Publishing Company, Amsterdam, 1962) P. 376.

9. W. L. Barr, J. Opt. Soc. Am. 52, 885 (1962).

10. K. Bockasten, J. Opt. Soc, Am. 51, 943 (1961).

11. H. Margenau and G. M. Murphy, The Mathematics of Physics and Chemistry, (D. Van Nostrand Company, Inc., Princeton, New Jersey, 1943) p. 507.

12. J. C. Van Den Bosch, The Zeeman Effect, (Handbuch der Physik, Springer - Verlag, 1956), Vol. XXVIII, p. 296.

13. S. Tolansky, High Resolution Spectroscopy, (Pitman Publishing Corp., New York, 1945), p. 138.

Appendix I

Manufacturing and Adjusting a Fabry-Perot Interferometer for Use in Near Red Spectrum

In order to observe certain near red Argon line shifts a Fabry-Perot interferometer was constructed to be used in the 7500-10,000Å region. Two 2-inch diameter fused silica plates with dielectric coatings were obtained from the Perkin-Elmer Corp. for the etalon. The transmittance of these plates are shown in figure 17. Various problems were incurred in manufacture and adjustment of the interferometer because of the very small reflectance in the visible spectrum. The most expeditious and sensitive solutions of these problems are reported here for future reference.

The housing for the etalon was fabricated in the physics department shop and is illustrated in figure 18. Two 2-inch diameter glass optical flats were coated with aluminum thin films by vacuum vaporization techniques to an overall reflectance of approximately 50%. A spacer was made by inserting three Invar pegs into a 2-inch diameter retaining ring at peripheral points corresponding to the pressure points of the interferometer housing. The pegs were ground on a surface plate until they were equal within 0.001" as measured with a micrometer. The interferometer was assembled with the aluminized plates and spacer. A low pressure mercury lamp was used as a light source to determine the need for further spacer grinding in order that the plates would be optically parallel. This determination was made by conventional methods and is outlined here.[13]

From the fringe pattern, the high point of the spacer can be

Figure 17

Reflectance of Plates Used in Fabry-Perot Interferometer

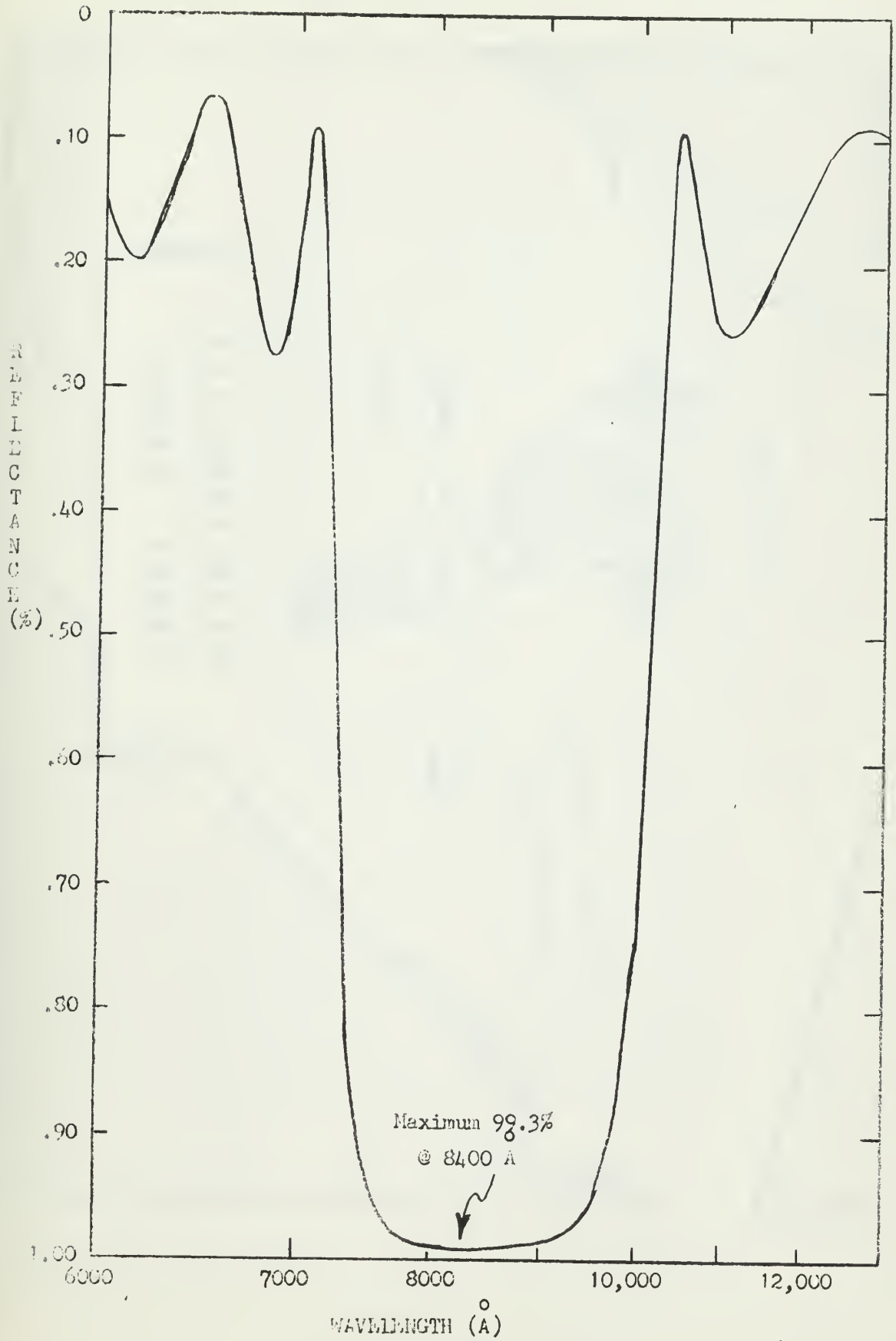

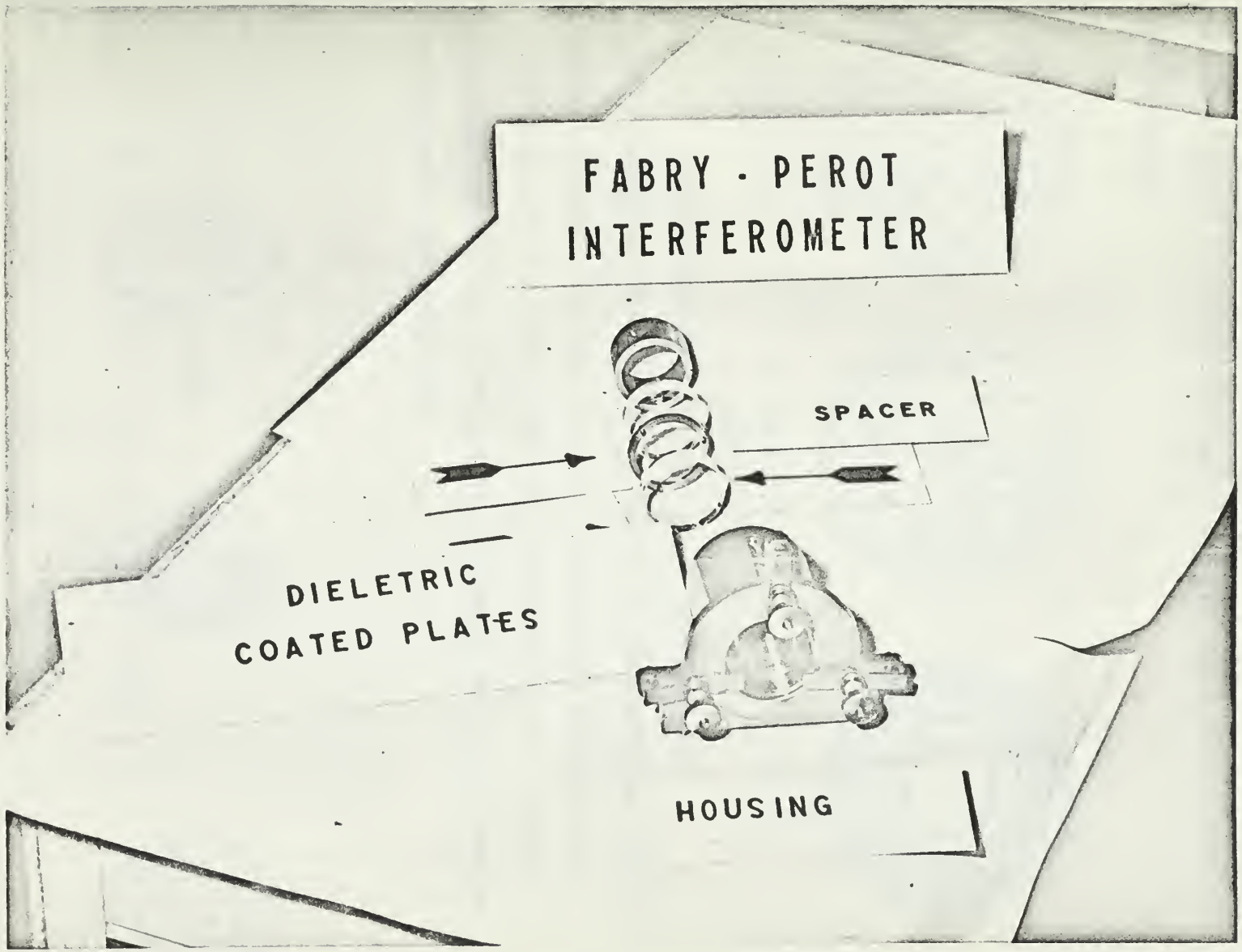
FABRY - PEROT
INTERFEROMETER
SPACER
DIELETRIC
COATED PLATES
HOUSING

Figure 13.

determined and the spacer subsequently ground to reduce the wedge angle. Figure 19 (a) shows a moderate degree of non-parallelism part (b) shows a reduce degree of non-parallelism, and part (c) shows nearly parallel plate pattern.

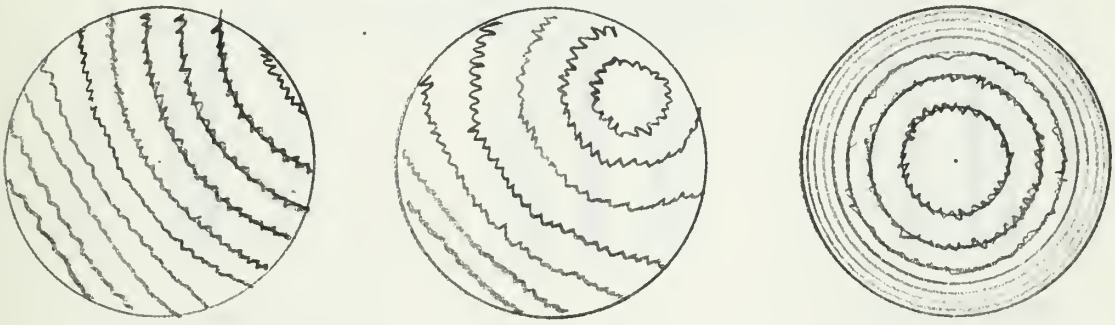

Part (a) Part (b) Part (c)

Figure 19

Course Adjustment of Fabry-Perot Interferometer

The final grinding is determined by moving the eye across the field of the interferometer. If the center most fringe opens when the eye is moved toward one peripheral point and closes when moved to the diametrically opposite point, the point toward which the fringe opens is the high point (see figure 20).

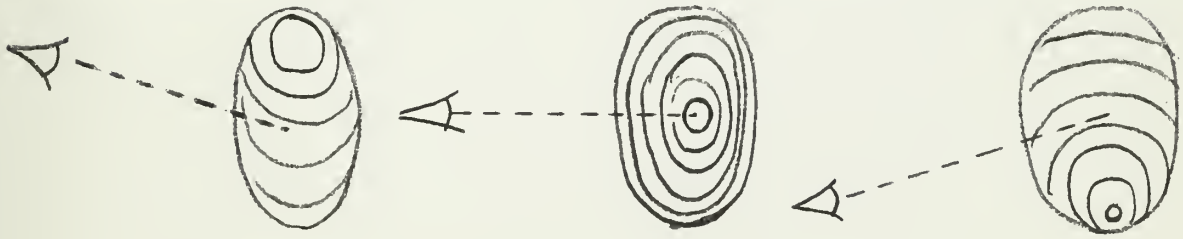

Figure 20

Fine Adjustment of Fabry-Perot Interferometer

However, a sensitive method of accomplishing this alignment was that of using the white light source at the plate holder and observing multiple reflections of the slit back on to the slit holder. Figure 21 illustrates this adjustment.

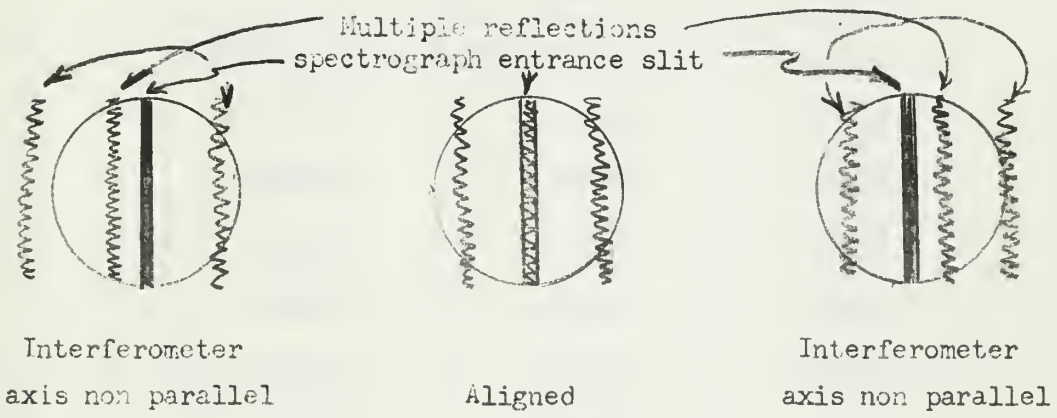

Figure 21

Centering of Fabry-Perot Pattern on Spectrograph

The interferometer was adjusted on the table so that the center reflection was coincident with the entrance slit of the spectrograph. A hard piece of "tacky wax" was placed around each foot of the interferometer prior to aligning. Once aligned, the wax was heated with a heat gun and then allowed to cool. This proved to be an excellent way of securing the interferometer against accidental jarring and at the same time did not disturb the interferometer alignment in the process.

APPENDIX II

TABLE 1

COMPARISON BETWEEN EXACT SOLUTION AND NUMERICAL METHOD SOLUTION

	I(x)	I(x)	ERROR
	FROM EQ (5.3)	FROM EQ (5.5)	%
1	1.000000	1.000000	0.0000
2	0.99248	0.99628	+0.3828
3	0.98496	0.98506	+0.0101
4	0.96241	0.96647	+0.4218
5	0.93984	0.94063	+0.0840
6	0.90977	0.90775	-0.2220
7	0.86466	0.86811	+0.3990
8	0.83458	0.82202	-1.5049
9	0.76692	0.76989	+0.3872
10	0.71428	0.71221	-0.2898
11	0.65413	0.64954	-0.8270
12	0.57969	0.58254	+0.4916
13	0.51127	0.51202	+0.1467
14	0.43985	0.43887	-0.0182
15	0.36842	0.36422	-1.1400
16	0.28947	0.28939	-0.0276
17	0.21804	0.21600	-0.9356
18	0.14586	0.14618	+0.2194
19	0.08271	0.08282	+0.1329
20	.03082	0.03044	-1.2337
21	0.00000	0.00000	0.0000

APPENDIX II

TABLE 2

CALCULATED INTENSITIES FROM ASSUMED RADIAL DISTRIBUTION

	CURVE 1		CURVE 2		CURVE 3		CURVE 4		CURVE 5	
j,K	E(r)	I(x)	E(r)	I(x)	E(r)	I(x)	E(r)	I(x)	E(r)	I(x)
1	1.0000	0.9933	1.0000	0.6287	1.0000	1.7146	1.0000	1.3333	1.0000	1.0021
2	0.9604	0.9828	0.9802	0.6163	1.0000	1.7117	0.9975	1.3283	0.9500	0.9909
3	0.9120	0.9575	0.9233	0.5807	1.0000	1.7029	0.9900	1.3134	0.9000	0.9662
4	0.8463	0.9218	0.8353	0.5257	1.0000	1.6881	0.9775	1.2886	0.8500	0.9315
5	0.8075	0.8816	0.7262	0.4573	1.0000	1.6672	0.9600	1.2541	0.8000	0.8890
6	0.7652	0.8336	0.6067	0.3823	1.0000	1.6399	0.9375	1.2103	0.7500	0.8401
7	0.7196	0.7788	0.4868	0.3068	1.0000	1.6059	0.9100	1.1574	0.7000	0.7860
8	0.6711	0.7183	0.3700	0.2365	1.0000	1.5647	0.8775	1.0960	0.6500	0.7278
9	0.6201	0.6532	0.2780	0.1767	1.0000	1.5159	0.8400	1.0265	0.6000	0.6664
10	0.5669	0.5847	0.1980	0.1263	1.0000	1.4585	0.7975	0.9496	0.5500	0.6027
11	0.5112	0.5140	0.1354	0.0869	1.0000	1.3915	0.7500	0.8660	0.5000	0.5373
12	0.4554	0.4423	0.0889	0.0580	1.0000	1.3134	0.6975	0.7767	0.4500	0.4711
13	0.3980	0.3707	0.0612	0.0374	1.0000	1.2219	0.6400	0.6827	0.4000	0.4049
14	0.3400	0.3005	0.0341	0.0217	1.0000	1.1136	0.5775	0.5851	0.3500	0.3395
15	0.2818	0.2330	0.0198	0.0126	1.0000	0.9818	0.5100	0.4856	0.3000	0.2756
16	0.2239	0.1698	0.0110	0.0070	0.9900	0.8138	0.4375	0.3858	0.2500	0.2143
17	0.1666	0.1123	0.0060	0.0037	0.9500	0.5805	0.3600	0.2880	0.2000	0.1566
18	0.1104	0.0626	0.0030	0.0018	0.6000	0.2702	0.2775	0.1949	0.1500	0.1038
19	0.0555	0.0234	0.0015	0.0009	0.1000	0.0409	0.1900	0.1104	0.1000	0.0577
20	0.0025	0.0010	0.0008	0.0003	0.0010	0.0004	0.0975	0.0406	0.0500	0.0208
21	0.0000	0.0000	0.0000	0.0000	0.0000	0.0000	0.0000	0.0000	0.0000	0.0000

APPENDIX II

TABLE 2 (CONTINUED)

	CURVE 6		CURVE 7		CURVE 8		CURVE 9		CURVE 10	
J,K	E(r)	I(x)	E(r)	I(x)	E(r)	I(x)	E(r)	I(x)	E(r)	I(x)
1	0.0000	0.9635	0.0000	0.8964	0.2000	0.9458	0.4000	0.9887	0.6000	1.0602
2	0.0000	0.9672	0.0200	0.9125	0.2100	0.9565	0.4100	0.9936	0.6050	1.0623
3	0.0000	0.9789	0.1700	0.9632	0.3000	0.9917	0.4200	1.0096	0.6350	1.0698
4	0.0000	0.9996	0.4350	1.0346	0.5000	1.0461	0.5000	1.0461	0.7000	1.0813
5	0.0000	1.0317	0.8000	0.0917	0.8000	1.0917	0.8000	1.0917	0.8000	0.0917
6	0.0000	1.0799	0.9500	1.0867	0.9500	1.0867	0.9500	1.0867	0.9500	1.0867
7	0.0000	1.1557	1.0000	1.0420	1.0000	1.0420	1.0000	1.0420	1.0000	1.0420
8	0.0000	1.3065	0.9950	0.9698	0.9950	0.9698	0.9950	0.9698	0.9950	0.9698
9	1.0000	1.5159	0.9800	0.8755	0.9800	0.8755	0.9800	0.8755	0.9800	0.8755
10	1.0000	1.4585	0.9150	0.7533	0.9150	0.7533	0.9150	0.7533	0.9150	0.7533
11	1.0000	1.3915	0.8000	0.6087	0.8000	0.6087	0.8000	0.6087	0.8000	0.6087
12	1.0000	1.3134	0.6000	0.4576	0.6000	0.4576	0.6000	0.4576	0.6000	0.4576
13	1.0000	1.2219	0.4450	0.3357	0.4450	0.3357	0.4450	0.3357	0.4450	0.3357
14	1.0000	1.1136	0.3200	0.2383	0.3200	0.2383	0.3200	0.2383	0.3200	0.2383
15	1.0000	0.9818	0.2300	0.1627	0.2300	0.1627	0.2300	0.1627	0.2300	0.1627
16	0.9900	0.8138	0.1500	0.1032	0.1500	0.1032	0.1500	0.1032	0.1500	0.1032
17	0.9500	0.5805	0.1000	0.0608	0.1000	0.0608	0.1000	0.0608	0.1000	0.0608
18	0.6000	0.2702	0.0500	0.0287	0.0500	0.0287	0.0500	0.0287	0.0500	0.0287
19	0.1000	0.0409	0.0200	0.0115	0.0200	0.0115	0.0200	0.0115	0.0200	0.0115
20	0.0010	0.0004	0.0100	0.0042	0.0100	0.0042	0.0100	0.0042	0.0100	0.0042
21	0.0000	0.0000	0.0000	0.0000	0.0000	0.0000	0.0000	0.0000	0.0000	0.0000

APPENDIX II

TABLE 2 (CONTINUED)

	CURVE 11		CURVE 12		CURVE 13		CURVE 14		CURVE 15	
J,K	E(r)	I(x)	E(r)	I(x)	E(r)	I(x)	E(r)	I(x)	E(r)	I(x)
1	0.8000	1.1257	1.0000	1.0447	0.1000	1.9504	1.0000	1.3159	1.0000	1.6174
2	0.8050	1.1242	1.0000	1.0395	1.0000	1.9479	1.0000	1.3119	1.0000	1.6143
3	0.8100	1.1192	1.0000	1.0236	1.0000	1.9401	1.0000	1.2999	1.0000	1.6048
4	0.8250	1.1114	1.0000	0.9964	1.0000	1.9272	1.0000	1.2795	1.0000	1.5890
5	0.8500	1.1017	1.0000	0.9563	1.0000	1.9090	1.0000	1.2504	1.0000	1.5664
6	0.9500	1.0867	1.0000	0.8997	1.0000	1.8852	1.0000	1.2116	1.0000	1.5370
7	1.0000	1.0420	0.9700	0.8202	1.0000	1.8558	1.0000	1.1620	1.0000	1.5001
8	0.9950	0.9698	0.8900	0.7189	1.0000	1.8204	1.0000	1.0992	1.0000	1.4553
9	0.9800	0.8755	0.7850	0.6048	1.0000	1.7788	1.0000	1.0181	1.0000	1.4016
10	0.9150	0.7533	0.6500	0.4840	1.0000	1.7303	0.9600	0.9115	1.0000	1.3378
11	0.8000	0.6087	0.5000	0.3682	1.0000	1.6745	0.8800	0.7841	1.0000	1.2622
12	0.6000	0.4576	0.3600	0.2696	1.0000	1.6105	0.7700	0.6434	1.0000	1.1718
13	0.4450	0.3357	0.2500	0.1942	1.0000	1.5374	0.6200	0.4978	1.0000	1.0602
14	0.3200	0.2383	0.1800	0.1402	1.0000	1.4538	0.4550	0.3667	0.9700	0.9166
15	0.2300	0.1627	0.1300	0.0989	1.0000	1.3577	0.3300	0.2651	0.8750	0.7396
16	0.1500	0.1032	0.0900	0.0607	1.0000	1.2462	0.2400	0.1872	0.7180	0.5448
17	0.1000	0.0608	0.0600	0.0429	1.0000	1.1146	0.1700	0.1264	0.5100	0.3583
18	0.0500	0.0287	0.0400	0.0257	1.0000	0.9547	0.1200	0.0793	0.3300	0.2103
19	0.0200	0.0115	0.0230	0.0127	1.0000	0.7478	0.0720	0.0412	0.1860	0.1028
20	0.0100	0.0042	0.0100	0.0042	1.0000	0.4163	0.0350	0.0146	0.0800	0.0333
21	0.0000	0.0000	0.0000	0.0000	0.0000	0.0000	0.0000	0.0000	0.0000	0.0000

APPENDIX II

TABLE 3

COMPARISON BETWEEN RADIAL DISTRIBUTION DETERMINED BY BARR AND BOCKASTEN METHODS

CURVE 1					
j	E(r)	E(r)*	ERROR*	E(r)**	ERROR**
1	1.0000	0.9595	-4.0470	1.0015	0.1470
2	0.9604	0.9483	-1.2568	0.9632	0.2926
3	0.9120	0.9153	0.3607	0.9124	0.0482
4	0.8463	0.8625	1.9201	0.8494	0.3639
5	0.8075	0.8144	0.8533	0.8081	0.0706
6	0.7652	0.7683	0.4038	0.7657	0.0601
7	0.7196	0.7230	0.4683	0.7200	0.0597
8	0.6711	0.6737	0.3859	0.6715	0.0596
9	0.6201	0.6232	0.5089	0.6205	0.0645
10	0.5669	0.5693	0.4322	0.5839	2.9970
11	0.5112	0.5143	0.6084	0.5117	0.0958
12	0.4554	0.4578	0.5292	0.4557	0.0703
13	0.3980	0.4007	0.6859	0.3984	0.1005
14	0.3400	0.3429	0.8588	0.3404	0.1206
15	0.2818	0.2846	1.0043	0.2822	0.1526
16	0.2239	0.2269	1.3354	0.2244	0.2144
17	0.1666	0.1698	1.9088	0.1672	0.3361
18	0.1104	0.1142	3.4783	0.1113	0.7880
19	0.0555	0.0643	15.9279	0.0552	-0.5225
20	0.0025	0.0276	-	0.0095	-
21	0.0000	0.0071	-	0.0000	0.0000

* BARR

** BOCKASTEN

APPENDIX II

TABLE 3 (CONTINUED)

CURVE 2					
j	E(r)	E(r)*	ERROR*	E(r)**	ERROR**
1	1.0000	0.9905	-0.9540	1.0010	0.0980
2	0.9802	0.9733	-0.6968	0.9813	0.1102
3	0.9233	0.9225	-0.0856	0.9243	0.1083
4	0.8353	0.8391	0.4621	0.8366	0.1568
5	0.7262	0.7355	1.2723	0.7278	0.2162
6	0.6067	0.6201	2.2105	0.6087	0.3412
7	0.4868	0.5030	3.3215	0.4883	0.3122
8	0.3700	0.3925	6.0728	0.3731	0.8297
9	0.2780	0.2954	6.2768	0.2797	0.6043
10	0.1980	0.2144	8.2862	0.2016	1.7875
11	0.1354	0.1505	11.1915	0.1368	1.0490
12	0.0890	0.1020	14.5971	0.0908	2.1014
13	0.0612	0.0667	9.0746	0.0612	0.1308
14	0.0341	0.0418	22.7633	0.0352	3.1974
15	0.0198	0.0249	25.6061	0.0203	2.3232
16	0.0110	0.0140	26.7452	0.0113	2.9918
17	0.0060	0.0077	28.7854	0.0062	2.9950
18	0.0030	0.0041	37.3333	0.0032	6.6667
19	0.0015	0.0021	38.6667	0.0014	-3.3333
20	0.0008	0.0009	26.6667	0.0007	-6.6667
21	0.0000	0.0004	-	0.0000	0.0000

* BARR

** BOCKASTEN

APPENDIX II

TABLE 3 (CONTINUED)

CURVE 3					
j	E(r)	E(r)*	ERROR*	E(r)**	ERROR**
1	1.0000	1.0018	0.1800	1.0000	0.0000
2	1.0000	1.0009	0.0870	1.0000	0.0000
3	1.0000	0.9996	-0.0370	1.0000	0.0000
4	1.0000	0.9976	-0.2380	1.0000	0.0000
5	1.0000	1.0000	0.0000	1.0000	0.0000
6	1.0000	1.0003	0.0300	1.0000	0.0000
7	1.0000	1.0012	0.1200	1.0000	0.0000
8	1.0000	0.9995	-0.0440	1.0000	0.0000
9	1.0000	1.0016	0.1600	1.0000	0.0000
10	1.0000	1.0005	0.0460	1.0550	5.4950
11	1.0000	1.0001	0.0160	0.9999	-0.0080
12	1.0000	0.9996	-0.0440	0.9998	-0.0160
13	1.0000	1.0000	0.0000	0.9996	-0.0360
14	1.0000	0.9987	-0.1310	0.9994	-0.0060
15	1.0000	0.9879	-1.2090	0.9975	-0.2470
16	0.9900	0.9395	-5.0990	0.9935	0.3545
17	0.9500	0.7981	-15.9916	0.9323	-1.8652
18	0.6000	0.5569	-7.1833	0.5833	-2.7833
19	0.1000	0.2924	192.4100	0.1327	32.7300
20	0.0010	0.0959	-	0.0147	-
21	0.0000	0.0120	-	0.0000	0.0000

* BARR

** BOCKASTEN

APPENDIX II

TABLE 3 (CONTINUED)

CURVE 4					
j	E(r)	E(r)*	ERROR*	E(r)**	ERROR**
1	1.0000	1.0008	0.0840	0.9999	-0.0090
2	0.9975	0.9978	0.0271	0.9975	0.0000
3	0.9900	0.9894	-0.0626	0.9900	0.0000
4	0.9975	0.9758	-0.1964	0.9975	0.0000
5	0.9600	0.9596	-0.0365	0.9600	0.0000
6	0.9375	0.9372	-0.0267	0.9375	0.0000
7	0.9100	0.9105	0.0516	0.9100	0.0000
8	0.8775	0.8769	-0.0627	0.8775	0.0000
9	0.8400	0.8407	0.0881	0.8400	0.0000
10	0.7975	0.7973	-0.0188	0.8282	3.8501
11	0.7500	0.7498	-0.0267	0.7500	0.0000
12	0.6975	0.6970	-0.0674	0.6975	0.0000
13	0.6400	0.6399	-0.0156	0.6400	0.0000
14	0.5775	0.5775	0.0000	0.5775	0.0000
15	0.5100	0.5095	-0.0863	0.5100	0.0000
16	0.4375	0.4372	-0.0594	0.4375	0.0000
17	0.3600	0.3598	-0.0500	0.3600	0.0000
18	0.2775	0.2775	0.0000	0.2775	0.0252
19	0.1900	0.1912	0.6421	0.1905	0.2684
20	0.0975	0.1090	11.8256	0.0936	-4.0308
21	0.0000	0.0467	-	0.0000	0.0000

* BARR

** BOCKASTEN

APPENDIX II

TABLE 3 (CONTINUED)

	CURVE 5				
	E(r)	E(r)*	ERROR *	E(r)**	ERROR**
1	1.0000	0.9490	-5.1040	1.0012	0.1190
2	0.9500	0.9384	-1.2158	0.9521	0.2210
3	0.9000	0.9075	0.8367	0.9010	0.1177
4	0.8500	0.8571	0.8412	0.8504	0.0529
5	0.8000	0.8070	0.8762	0.8001	0.0137
6	0.7500	0.7560	0.7960	0.7498	-0.0307
7	0.7000	0.7056	0.8057	0.6994	-0.0900
8	0.6500	0.6543	0.6662	0.6488	-0.1815
9	0.6000	0.6046	0.7683	0.5992	-0.1333
10	0.5500	0.5536	0.6582	0.5497	-0.0491
11	0.5000	0.5033	0.6580	0.5250	5.0000
12	0.4500	0.4528	0.6333	0.4531	0.6867
13	0.4000	0.0428	0.7075	0.4003	0.0800
14	0.3500	0.3527	0.7600	0.3503	0.0857
15	0.3000	0.3022	0.7467	0.3003	0.0900
16	0.2500	0.2522	0.8760	0.2502	0.1000
17	0.2000	0.2021	1.0500	0.2002	0.1200
18	0.1500	0.1521	1.3867	0.1502	0.1667
19	0.1000	0.1026	2.5600	0.1004	0.4500
20	0.0500	0.0574	14.9800	0.0483	-3.3000
21	0.0000	0.0243	-	0.0000	0.0000

* BARR

** BOCKASTEN

APPENDIX II

TABLE 3 (CONTINUED)

CURVE 6					
j	E(r)	L(r)*	ERROR*	E(r)**	ERROR**
1	0.0000	0.0012	-	-0.0028	-
2	0.0000	0.0006	-	0.0023	-
3	0.0000	-0.0001	-	0.0005	-
4	0.0000	-0.0019	-	0.0006	-
5	0.0000	0.0004	-	0.0014	-
6	0.0000	0.0095	-	0.0063	-
7	0.0000	0.0858	-	0.00273	-
8	0.0000	0.3173	-	0.0895	-
9	1.0000	0.6215	-37.8480	0.9174	-8.2640
10	1.0000	0.8810	-11.9040	1.0550	5.4950
11	1.0000	1.0001	0.0160	1.0000	0.0000
12	1.0000	0.9996	-0.0440	0.9998	-0.0160
13	1.0000	1.0000	0.0000	0.9996	-0.0360
14	1.0000	0.9987	-0.1310	0.9994	-0.0580
15	1.0000	0.9879	-1.2090	0.9975	-0.2470
16	0.9900	0.9395	-5.0990	0.9935	0.3545
17	0.9500	0.7981	-15.9916	0.9323	-1.8652
18	0.6000	0.5569	-7.1833	0.5833	-2.7833
19	0.1000	0.2924	192.4100	0.1327	32.7300
20	0.0010	0.0959	-	0.0147	-
21	0.0000	0.0120	-	0.0000	0.0000

* BARR

** BOCKASTEN

APPENDIX II

TABLE 3 (CONTINUED)

CURVE 7					
j	E(r)	E(r)*	ERROR*	E(r)**	ERROR*
1	0.0000	-0.0155	-	-0.0023	-
2	0.0200	0.0339	69.7000	0.0178	-11.0500
3	0.1700	0.1819	7.0000	0.1648	-3.0529
4	0.4350	0.4196	-3.5402	0.4366	0.3586
5	0.8000	0.6746	-15.6750	0.7811	-2.3662
6	0.9500	0.8636	-9.0958	0.9418	-0.8631
7	1.0000	0.9601	-3.9900	0.9951	-0.4890
8	0.9950	0.9790	-1.6030	0.9947	-0.0271
9	0.9800	0.9535	-2.7010	0.9769	-0.3133
10	0.9150	0.8838	-3.4098	0.9291	1.5387
11	0.8000	0.7700	-3.7413	0.7941	-0.7400
12	0.6000	0.6249	4.1500	0.6047	0.7833
13	0.4450	0.4760	6.9753	0.4479	0.6427
14	0.3200	0.3469	8.4062	0.3236	1.1187
15	0.2300	0.2461	6.9913	0.2308	0.3478
16	0.1500	0.1683	12.2133	0.1530	1.9867
17	0.1000	0.1081	8.1500	0.1000	0.0000
18	0.0500	0.0632	26.4600	0.0514	2.9200
19	0.0200	0.326	63.0000	0.0218	8.8500
20	0.0100	0.0138	38.4000	0.0097	-3.4000
21	0.0000	0.0048	-	0.0000	0.0000

*BARR

** BOCKASTEN

APPENDIX II

TABLE 3 (CONTINUED)

CURVE 8					
j	E(r)	E(r)*	ERROR*	E(r)**	ERROR**
1	0.2000	0.1668	-16.1100	0.1992	-0.3850
2	0.2100	0.2052	-2.2714	0.2084	-0.7476
3	0.3000	0.3173	5.7667	0.2974	-0.8633
4	0.5000	0.4985	-0.2860	0.5020	0.3920
5	0.8000	0.7070	-11.6275	0.7864	-1.7050
6	0.9500	0.8711	-8.3011	0.9417	-0.8737
7	1.000	0.9601	-3.9900	0.9951	-0.4900
8	0.9950	0.9790	-1.6030	0.9947	-0.0271
9	0.9800	0.9535	-2.7010	0.9769	-0.3133
10	0.9150	0.8838	-3.4098	0.9291	1.5388
11	0.8000	0.7700	-3.7413	0.7941	-0.7400
12	0.6000	0.6249	4.1500	0.6047	0.7833
13	0.4450	0.4760	6.9753	0.4479	0.6427
14	0.3200	0.3469	8.4000	0.3236	1.1187
15	0.2300	0.2461	6.9913	0.2308	0.3478
16	0.1500	0.1683	12.2133	0.1530	1.9867
17	0.1000	0.1081	8.1500	0.1000	0.0000
18	0.0500	0.0632	26.4600	0.0514	2.9200
19	0.0200	0.0326	63.0000	0.0218	8.8500
20	0.0100	0.0138	38.4000	0.0097	-3.4000
21	0.0000	0.0048	-	0.0000	0.0000

* BARR*

** BOCKASTEN

APPENDIX II

TABLE 3 (CONTINUED)

CURVE 9					
j	E(r)	E(r)*	ERROR*	E(r)**	ERROR**
1	0.4000	0.3484	-12.8900	0.4009	0.2275
2	0.4100	0.3709	-9.5268	0.4103	0.0829
3	0.4200	0.4382	4.3357	0.4164	-0.8548
4	0.5000	0.5519	10.3840	0.5114	2.2740
5	0.8000	0.7203	-9.9588	0.7863	-1.7150
6	0.9500	0.8711	-8.3011	0.9418	-0.8631
7	1.0000	0.9601	-3.9900	0.9951	-0.4890
8	0.9950	0.9790	-1.6030	0.9947	-0.0271
9	0.9800	0.9535	-2.7010	0.9769	-0.3133
10	0.9150	0.8838	-3.4098	0.9290	1.5388
11	0.8000	0.7700	-3.7413	0.7941	-0.7400
12	0.6000	0.6249	4.1500	0.6047	0.7833
13	0.4450	0.4760	6.9753	0.4479	0.6427
14	0.3200	0.3469	8.4000	0.3236	1.1187
15	0.2300	0.2461	6.9913	0.2308	0.3478
16	0.1500	0.1683	12.2133	0.1530	1.9867
17	0.1000	0.1081	8.1510	0.1000	0.0000
18	0.0500	0.0632	26.4600	0.0515	2.9200
19	0.0200	0.0326	63.0000	0.0218	8.8000
20	0.0100	0.0138	38.4000	0.0097	-3.4000
21	0.0000	0.0048	-	0.0000	0.0000

* BARR

** BOCKASTEN

APPENDIX II

TABLE 3 (CONTINUED)

CURVE 10					
j	E(r)	E(r)*	ERROR*	E(r)**	ERROR**
1	0.6000	0.5888	-1.8700	0.5996	-6.7317
2	0.6060	0.6016	-0.5570	0.6044	-0.0926
3	0.6350	0.6401	0.8016	0.6346	-0.0567
4	0.7000	0.7048	0.6843	0.6980	-0.2886
5	0.8000	0.7994	-0.0763	0.8021	0.2675
6	0.9500	0.8944	-5.8516	0.9416	-0.8821
7	1.0000	0.9601	-3.9900	0.9949	-0.5080
8	0.9950	0.9790	-1.6030	0.9945	-0.0492
9	0.9800	0.9535	-2.7010	0.9767	-0.3377
10	0.9150	0.8838	-3.4098	0.9288	1.5082
11	0.8000	0.7700	-3.7413	0.7937	-0.7812
12	0.6000	0.6249	4.1500	0.6043	0.7150
13	0.4450	0.4760	6.9753	0.4473	0.5213
14	0.3200	0.3469	8.4000	0.3228	0.8750
15	0.2300	0.2461	6.9913	0.2302	0.0913
16	0.1500	0.1683	12.2133	0.1438	-4.1400
17	0.1000	0.1081	8.1500	0.1123	12.3400
18	0.0500	0.0632	26.4600	0.0528	5.6800
19	0.0200	0.0326	63.0000	0.0218	8.8500
20	0.0100	0.0138	38.4000	0.0097	-3.4000
21	0.0000	0.0048	-	0.0000	0.0000

* BARR

** BOCKASTEN

APPENDIX II

TABLE 3 (CONTINUED)

CURVE 11					
j	E(r)	E(r)*	ERROR*	E(r)**	ERROR**
1	0.8000	0.7985	-0.1813	0.8000	0.0000
2	0.8050	0.8018	-0.4025	0.8048	-0.0285
3	0.8100	0.8014	0.1778	0.8105	0.0654
4	0.8250	0.8294	0.5394	0.8230	-0.2364
5	0.8500	0.8700	2.4529	0.8543	0.5178
6	0.9200	0.9225	-2.8989	0.9458	-0.4358
7	1.0000	0.9660	-3.3980	0.9951	-0.4890
8	0.9950	0.9790	-1.6030	0.9947	-0.0271
9	0.9800	0.9535	-2.7010	0.9769	-0.3133
10	0.9150	0.8838	-3.4098	0.9291	1.5388
11	0.8000	0.7700	-3.7413	0.7941	-0.7400
12	0.6000	0.6249	4.1500	0.6047	0.7833
13	0.4450	0.4760	6.9753	0.4479	0.6427
14	0.3200	0.3469	8.4000	0.3236	1.1187
15	0.2300	0.2461	6.9913	0.2308	0.3478
16	0.1500	0.1683	12.2133	0.1530	1.9867
17	0.1000	0.1081	8.1500	0.1000	0.0000
18	0.0500	0.0632	26.4600	0.0514	2.9200
19	0.0200	0.0326	63.0000	0.0218	8.8500
20	0.0100	0.0138	38.40000	0.0097	-3.4000
21	0.0000	0.0048	-	0.0000	0.0000

* BARR

** BOCKASTEN

APPENDIX II

TABLE 3 (CONTINUED)

CURVE 12					
j	E(r)	E(r)*	ERROR*	E(r)**	ERROR**
1	1.0000	1.0008	0.0800	0.9998	-0.0230
2	1.0000	1.0005	0.0500	0.9998	-0.0220
3	1.0000	-0.0190	0.9998	-0.0240	-0.0470
4	1.0000	0.9989	-0.1130	0.9995	-0.0470
5	1.0000	0.9972	-0.2790	1.0000	0.0000
6	1.0000	0.9837	-1.6340	0.9986	-0.1360
7	0.9700	0.9473	-2.3422	0.9672	-0.2897
8	0.8900	0.8777	-1.3798	0.8897	-0.0371
9	0.7850	0.7768	-1.0433	0.7844	-0.0802
10	0.6500	0.6510	0.1523	0.6590	1.3892
11	0.5000	0.5160	3.1940	0.5018	0.3600
12	0.3600	0.3871	7.5222	0.3628	0.7694
13	0.2500	0.2795	11.7960	0.2536	1.4280
14	0.1800	0.1984	10.2222	0.1819	1.0611
15	0.1300	0.1403	7.9615	0.1310	0.7538
16	0.0900	0.0985	9.5000	0.0908	0.9333
17	0.0600	0.0673	12.1667	0.0609	1.5333
18	0.0400	0.0438	9.5750	0.0403	0.7250
19	0.0230	0.0263	14.1739	0.0234	1.7391
20	0.0100	0.0134	34.2000	0.0101	0.8000
21	0.0000	0.0052	-	0.0000	0.0000

* BARR

** BOCKASTEN

APPENDIX II

TABLE 3 (CONTINUED)

CURVE 13					
j	E(r)	E(r)*	ERROR*	E(r)**	ERROR*
1	1.0000	1.0019	0.1900	0.9994	-0.0560
2	1.0000	1.0009	0.0900	0.9994	-0.0620
3	1.0000	0.9995	-0.0500	0.9993	-0.0650
4	1.0000	0.9975	-0.2500	0.9993	-0.0660
5	1.0000	1.0000	0.0000	0.9993	-0.0650
6	1.0000	1.0003	0.0300	0.9993	-0.0700
7	1.0000	1.0012	0.1270	0.9993	-0.0740
8	1.0000	0.9994	-0.0600	0.9992	-0.0770
9	1.0000	1.0025	0.2460	0.9992	-0.0830
10	1.0000	1.0007	0.0740	1.0683	6.8270
11	1.0000	1.0003	0.0310	0.9990	-0.0980
12	1.0000	0.9996	-0.0360	0.9989	-0.1130
13	1.0000	1.0007	0.0670	0.9987	-0.1310
14	1.0000	1.0007	0.0720	0.9984	-0.1550
15	1.0000	0.9996	-0.0370	0.9980	-0.1970
16	1.0000	0.9998	-0.0200	0.9973	-0.2650
17	1.0000	0.9995	-0.0520	0.9959	-0.4120
18	1.0000	0.9883	-1.1670	0.9898	-1.0210
19	1.0000	0.9001	-9.9900	1.0183	1.8270
20	1.0000	0.6633	-33.6690	0.8269	-17.3080
21	0.0000	0.3680	-	0.0000	0.0000

* BARR

** BOCKASTEN

APPENDIX II

TABLE 3 (CONTINUED)

CURVE 14					
j	E(r)	E(r)*	ERROR*	E(r)**	ERROR**
1	1.0000	1.0011	0.1110	0.9995	-0.0050
2	1.0000	1.0007	0.0670	0.9998	-0.0140
3	1.0000	0.9998	-0.0230	0.9999	0.0080
4	1.0000	0.9985	-0.1530	0.9999	-0.0060
5	1.0000	0.9999	-0.0050	0.9998	-0.0150
6	1.0000	0.9999	-0.0090	0.9998	-0.0190
7	1.0000	1.0003	0.0270	0.9995	-0.0530
8	1.0000	0.9953	-0.4660	1.0003	0.0280
9	1.0000	0.9795	-2.0500	0.9795	0.0000
10	0.9600	0.9373	-2.3677	0.9801	2.0896
11	0.8800	0.8631	-1.9239	0.8792	-0.0954
12	0.7700	0.7543	-2.0403	0.7685	-0.1948
13	0.6200	0.6218	0.2935	0.6195	-0.0855
14	0.4550	0.4835	6.2571	0.4587	0.8088
15	0.3300	0.3585	8.6333	0.3332	0.9818
16	0.2400	0.2593	8.0292	0.2417	0.7167
17	0.1700	0.1846	8.5941	0.1720	1.1647
18	0.1200	0.1266	5.4833	0.1202	0.1833
19	0.0720	0.0797	10.6806	0.0732	1.6944
20	0.0350	0.0425	21.3714	0.0341	-2.5142
21	0.0000	0.0172	-	0.0000	0.0000

* BARR

** BCCKASTEN

APPENDIX II

TABLE 3 (CONTINUED)

CURVE 15					
j	E(r)	E(r)*	ERROR*	E(r)**	ERROR**
1	1.0000	1.0016	0.1610	0.9999	-0.0130
2	1.0000	1.0008	0.0810	0.9999	-0.0030
3	1.0000	0.9997	-0.0330	1.0000	0.0000
4	1.0000	0.9978	-0.2230	0.9999	-0.0030
5	1.0000	0.9999	-0.0050	0.9999	-0.0030
6	1.0000	1.0002	0.0190	0.9999	-0.0030
7	1.0000	1.0010	0.0130	0.9999	-0.0030
8	1.0000	0.9996	-0.0420	0.9999	-0.0030
9	1.0000	1.0014	0.1420	0.9999	-0.0030
10	1.0000	1.0003	0.0270	1.0475	4.7480
11	1.0000	0.9996	-0.0350	0.9995	-0.0500
12	1.0000	0.9955	-0.4440	0.9998	-0.0160
13	1.0000	0.9791	-2.0890	0.9984	-0.1640
14	0.9700	0.9322	-3.9000	0.9660	-0.4082
15	0.8750	0.8387	-4.1486	0.8721	-0.3360
16	0.7180	0.6985	-2.7159	0.7147	-0.4512
17	0.5100	0.5298	3.8804	0.5130	0.5843
18	0.3300	0.3614	9.5121	0.3333	0.9970
19	0.1860	0.2168	16.5430	0.1896	1.9624
20	0.0800	0.1090	36.2875	0.0810	1.2375
21	0.0000	0.0419	-	0.0000	0.0000

* BARR

** BOCKASTEN